

การเร่งปฏิบัติการแบบใช้แสงร่วมในการย่อยสลายสารละลาย 2,4-ไดคลอโรฟีนอล ภายใต้การฉาย  
แสงขาวโดยใช้ตัวเร่งปฏิกิริยาไทเทเนียมไดออกไซด์ที่กระตุ้นด้วยโลหะเงินซึ่งสังเคราะห์โดยใช้  
โพลีเอธิลีนไกลคอลเป็นแม่แบบ



นางสาวสินีนฏ อันบุรี

ศูนย์วิทยทรัพยากร  
จุฬาลงกรณ์มหาวิทยาลัย

วิทยานิพนธ์นี้เป็นส่วนหนึ่งของการศึกษาตามหลักสูตรปริญญาวิทยาศาสตรมหาบัณฑิต

สาขาวิชาการจัดการสิ่งแวดล้อม (สหสาขาวิชา)

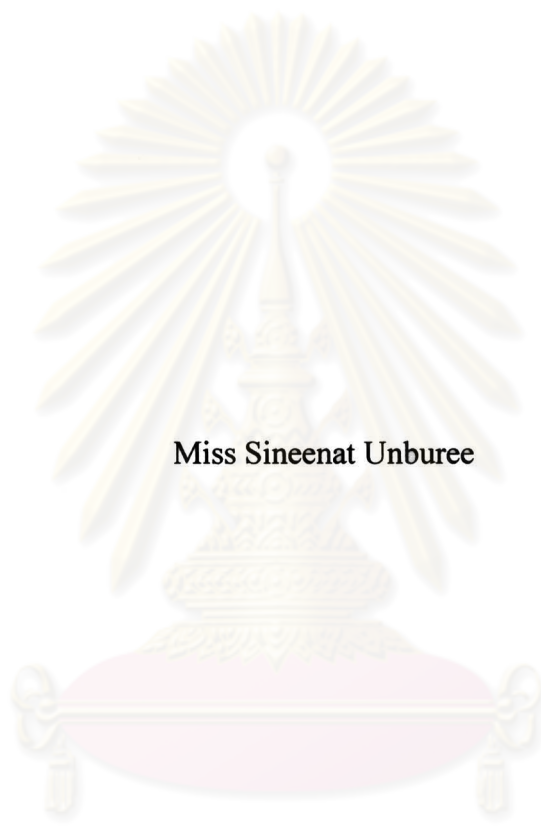
บัณฑิตวิทยาลัย จุฬาลงกรณ์มหาวิทยาลัย

ปีการศึกษา 2552

ลิขสิทธิ์ของจุฬาลงกรณ์มหาวิทยาลัย

**521194**

**PHOTODEGRADATION OF 2,4-DICHLOROPHENOL IN AQUEOUS SOLUTION  
UNDER VISIBLE LIGHT BY SILVER DOPED TITANIUM DIOXIDE  
SYNTHESIZED BY USING POLYEHTYLENE GLYCOL AS TEMPLATE**



**Miss Sineenat Unburee**

**ศูนย์วิทยทรัพยากร  
จุฬาลงกรณ์มหาวิทยาลัย**

**A Thesis Submitted in Partial Fulfillment of the Requirements  
for the Degree of Master of Science Program in Environmental Management  
(Interdisciplinary Program)  
Graduate School  
Chulalongkorn University  
Academic Year 2009**

**Copyright of Chulalongkorn University**

Thesis Title           **PHOTODEGRADATION OF 2,4-DICHLOROPHENOL  
IN AQUEOUS SOLUTION UNDER VISIBLE LIGHT  
BY SILVER DOPED TITANIUM DIOXIDE  
SYNTHESIZED BY USING POLYEHTYLENE  
GLYCOL AS TEMPLATE**

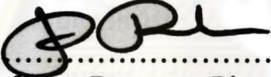
By                       Miss Sineenat Unburee

Field of Study        Environmental Management

Thesis Advisor       Associate Professor Nurak Grisdanurak, Ph.D.

---


Accepted by the Graduate School, Chulalongkorn University in Partial  
Fulfillment of the Requirements for the Master's Degree


  
..... Dean of the Graduate School  
(Associate Professor Pornpote Piumsomboon, Ph.D.)

THESIS COMMITTEE

  
..... Chairman  
(Assistant Professor Manaskorn Rachakornkij, Ph.D.)

  
..... Thesis Advisor  
(Associate Professor Nurak Grisdanurak, Ph.D.)

  
..... Examiner  
(Associate Professor Jin Anotai, Ph.D.)

  
..... Examiner  
(Assistant Professor Khemarath Osathaphan, Ph.D.)

  
..... External Examiner  
(Panjai Saueprasearsit, Ph.D.)

---

สินีนานู อ้นบุรี : การเร่งปฏิกิริยาแบบใช้แสงร่วมในการย่อยสลายสารละลาย 2,4-ไดคลอโรฟีนอล ภายใต้การฉายแสงขาวโดยใช้ตัวเร่งปฏิกิริยาไทเทเนียมไดออกไซด์ที่กระตุ้นด้วยโลหะเงินซึ่งสังเคราะห์โดยใช้โพลีเอทิลีนไกลคอลเป็นแม่แบบ. (PHOTODEGRADATION OF 2,4-DICHLOROPHENOL IN AQUEOUS SOLUTION UNDER VISIBLE LIGHT BY SILVER DOPED TITANIUM DIOXIDE SYNTHESIZED BY USING POLYEHTYLENE GLYCOL AS TEMPLATE.)  
 อ. ที่ปรึกษาวิทยานิพนธ์หลัก : รศ.ดร. นุรักษ์ กฤษดาบุรุษย์, 57 หน้า.

การวิจัยนี้มีวัตถุประสงค์เพื่อศึกษา ตัวเร่งปฏิกิริยาไทเทเนียมไดออกไซด์ที่กระตุ้นด้วยโลหะเงิน ( $\text{Ag-TiO}_2$ ) ถูกสังเคราะห์โดยใช้ Titanium Tetraisopropoxide (TTIP) และ โพลีเอทิลีนไกลคอล (PEG) เป็นแม่แบบและเตรียมด้วยวิธีโซลเจล ตัวเร่งปฏิกิริยาจะถูกตรวจสอบคุณลักษณะทั้งทางเคมีและกายภาพ รวมทั้งการทดสอบประสิทธิภาพของตัวเร่งปฏิกิริยาแต่ละตัวภายใต้การฉายแสงขาว การออกแบบการทดลองเชิงสถิติแบบ Box-Behnken design ศึกษา 3 ปัจจัยที่มีผลต่อประสิทธิภาพในการย่อยสลายสาร 2,4-DCP คือ ปริมาณ PEG ปริมาณตัวเร่งปฏิกิริยา และความเข้มข้นของ  $\text{K}_2\text{S}_2\text{O}_8$  พบว่าสถานะที่ดีที่สุดในการย่อยสลาย 2,4-DCP คือ ตัวเร่งปฏิกิริยาที่ไม่ใช่ PEG ในการสังเคราะห์ ในสัดส่วน 1 กรัมต่อลิตรของสารละลาย ภายใต้ความเข้มข้นของ  $\text{K}_2\text{S}_2\text{O}_8$  0.15 มิลลิโมลาร์และอัตราการเกิดปฏิกิริยาสามารถอธิบายได้ตามรูปแบบการเกิดปฏิกิริยาแบบแลงเมียร์-ฮินเชอว์วูด

ศูนย์วิทยทรัพยากร  
 จุฬาลงกรณ์มหาวิทยาลัย

สาขาวิชา การจัดการสิ่งแวดล้อม ..... ลายมือชื่อนิสิต ..... สินีนานู อ้นบุรี .....  
 ปีการศึกษา 2552 ..... ลายมือชื่อ อ.ที่ปรึกษาวิทยานิพนธ์หลัก ..... 



# # 5187593720 : MAJOR ENVIRONMENTAL MANAGEMENT

KEYWORDS : Ag-TiO<sub>2</sub> / PHOTODEGRADATION / 2,4-DCP / PEG / BOX-BEHNKEN / K<sub>2</sub>S<sub>2</sub>O<sub>8</sub>

SINEENAT UNBUREE: PHOTODEGRADATION OF 2,4-DICHLOROPHENOL IN AQUEOUS SOLUTION UNDER VISIBLE LIGHT BY SILVER DOPED TITANIUM DIOXIDE SYNTHESIZED BY USING POLYEHTYLENE GLYCOL AS TEMPLATE. THESIS  
ADVISOR: ASSOC. PROF. NURAK GRISDANURAK, Ph.D., 57 pp.

In this study, Ag-TiO<sub>2</sub> photocatalysts were prepared via sol-gel method by using Titanium Tetraisopropoxide (TTIP) and polyethylene glycol (PEG) as precursor and template respectively. The synthesized catalysts were characterized by several techniques for their physico-chemical properties. Furthermore, catalysts were tested on the photocatalytic degradation of 2,4-DCP under visible light irradiation. Box-Behnken experimental design was applied to determine the optimum condition of the photocatalytic degradation of 2,4-DCP. Three factors including, PEG content, photocatalyst loading, and concentration of K<sub>2</sub>S<sub>2</sub>O<sub>8</sub>, were investigated. PEG did not affect to photocatalytic degradation of 2,4-DCP. The best condition was obtained at Ag-TiO<sub>2</sub> prepared without PEG, loading of 0.1 g/L, and 0.15 mM of K<sub>2</sub>S<sub>2</sub>O<sub>8</sub>. The reaction rate can be expressed by Langmiur-Hinshewood (LHHW) model.

ศูนย์วิทยทรัพยากร  
จุฬาลงกรณ์มหาวิทยาลัย

Field of Study : Environmental Management

Academic Year : 2009

Student's Signature สินธุ คุ้ม

Advisor's Signature นุระก

## ACKNOWLEDGEMENTS

I would like to express my sincere gratitude to the following people for offering my great support and encouragement during my valuable year of Master study. Firstly, I would like to gratefully acknowledge my thesis advisor, Associate Professor Dr. Nurak Grisdanurak for his invaluable support and kind guidance throughout my work. Comments and suggestions from my advisor let me see the way to develop thinking skills.

My gratitude goes to the National Center of Excellence for Environmental and Harzard Waste Management (NCE-EHWM) for giving my opportunity to study in International Postgraduate Programs in Environmental Management. I also gratefully acknowledge Asst. Professor Dr. Manaskorn Rachakornkij, Asst. Prof. Dr. Jin Anotai, and Asst. Prof. Dr. Khemarath Osathaphan, Dr. Panjai Saueprasearsit, Dr. Chantra Tongcumpou, Dr. nyein nyein aung, and Dr. Pichet Chivivatvorakul thesis committees for fruitful comments and advices.

Special gratitude goes to Dr. Pongthanawat Khemthong, post doctoral student, for his gratitude advice and revise my thesis proposal and defense examinations, Mr. Kitirote Wantala, Ph.D. student, for his teaching , and helpful guildance meant for the experiment throughout my work, Ajarn Laksana laokiat, Ph.D. student, for giving me kindness advices and support, Ms. Pummarin Khamdahsag, Ph.D. student, for her help, advices, and encouragement during my research, Mr. Danutawat Tipayarom Ph.D. student for giving advice and experimental support, and thank to all member in catalyst lab at Department of Chemmical Engineering, Thammasart University for kindness relationship. I also thank Synchrotron Light Research Institute (Public organization), Nakorn Ratchasima, Thailand for XAS technique support.

Finally, I am also greatly indebted to my parents; Mr.Suree and Mrs.Rujira Unburee for giving me life, for their greatest love and understanding.

# CONTENTS

	Page
ABSTRACT (IN THAI).....	iv
ABSTRACT (IN ENGLISH).....	v
ACKNOWLEDGEMENTS.....	vi
CONTENTS.....	vii
LIST OF TABLES.....	xi
LIST OF FIGURES.....	xiii
CHAPTER I : INTRODUCTION	
1.1 Motivation.....	1
1.2 Objectives.....	3
1.3 Scope of Study.....	4
1.4 Expected Outcomes.....	4
CHAPTER II : LITERATURE REVIEW	
2.1 Chlorophenols (CPs).....	5
2.1.1 General information of chlorophenols (CPs).....	5
2.1.2 Use of 2,4-dichlorophenol.....	6
2.1.3 Environmental standards for 2,4-DCP.....	7



2.1.4 Environmental and health concern on 2,4-DCP.....	7
2.2 Basic principles of photocatalysis.....	8
2.2.1 Titanium dioxide photocatalys.....	10
2.2.2 Photocatalytic reaction of TiO <sub>2</sub> .....	11
2.2.3 Photocatalyst preparation by sol-gel method.....	12
2.2.4 Surface modification of TiO <sub>2</sub> by metal doping.....	13
2.2.5 Addition of polyethylene glycol (PEG) as template.....	13

### CHAPTER III : MATERIALS AND METHODS

3.1 Materials.....	15
3.2 Photocatalys preparation.....	15
3.3 Photocatalyst characterization.....	16
3.3.1 Thermogravimatic-differential thermogravimatic analysis (TG-DTA)..	16
3.3.2 X-ray diffraction (XRD).....	16
3.3.3 UV-vis diffuse reflectance spectroscopy (UV-DRS).....	16
3.3.4 Brunauer-Emmett-Teller (BET) method.....	17
3.3.5 Scanning electron microscopy (SEM).....	17
3.3.6 X-ray absorption spectroscopy (XAS).....	17
3.3.7 Zeta potential technique.....	17
3.4 Photocatalytic study.....	18

3.5 Analytical method.....	19
----------------------------	----

## CHAPTER IV : RESULTS AND DISCUSSIONS

4.1 Characterization results.....	20
4.1.1 Thermoanalysis by TG-DTA.....	20
4.1.2 Surface morphology of photocatalysts by SEM.....	21
4.1.3 Determination of crystalline size of photocatalysts by XRD.....	22
4.1.4 Determination visible light adsorption capacity by UV-DRS.....	23
4.1.5 Zeta potential technique.....	25
4.1.6 Determination specific surface area by BET method.....	26
4.1.7 X-ray absorption spectroscopy (XAS).....	27
4.2 Photocatalytic study.....	28
4.2.1 Determination of $K_2S_2O_8$ ranges.....	28
4.2.2 Factor evaluation on photocatalytic degradation of 2,4-DCP by Box- Behnken design.....	29
4.3 Photocatalytic testing.....	37
4.3.1 Determination the effect of initial concentration.....	37
4.3.2 Kinetic model of photocatalytic degradation of 2,4-DCP.....	39
4.3.3 Determination the effect of the $K_2S_2O_8$ addition.....	41

## CHAPTER V: CONCLUSIONS AND RECCOMENDATIONS

5.1 Conclusions.....	44
----------------------	----



5.2 Recommendations.....	45
REFERENCES.....	46
APPENDIX.....	51
1. Determination of energy band gap from absorption coefficient by Kubelka Munk Model.....	52
2. Determination of point of zero charge from Zeta potential.....	53
3. Calibration curve of 2,4-DCP.....	54
4. Kinetic study.....	55
BIOGRAPHY.....	57



ศูนย์วิทยทรัพยากร  
จุฬาลงกรณ์มหาวิทยาลัย

## LIST OF TABLES

<b>Table</b>		<b>Page</b>
2.1	Chemical and physical properties of 2,4-DCP.....	6
4.1	Average crystalline size of samples.....	23
4.2	Energy band gap of Ag-TiO <sub>2</sub> samples.....	24
4.3	Zeta potential of different PEG content in photocatalyst suspension...	25
4.4	BET surface area of each Ag-TiO <sub>2</sub> samples.....	26
4.5	Range and levels of Box-Behnken design with three factors.....	29
4.6	Design matrix and results of Box-Behnken design.....	30
4.7	Estimated regression coefficients for %removal of 2,4-DCP.....	32
4.8	Degradation of 2,4-DCP under different conditions.....	42
A.1	Zeta potential results of Ag-TiO <sub>2</sub> with difference mol% of PEG.....	53
A.2	Different concentrations were obtained from peak area analyzed by HPLC for calibration curve of 2,4-DCP.....	54
A.3	Determination the concentration of K <sub>2</sub> S <sub>2</sub> O <sub>8</sub> analyzed by HPLC for photodcatalytic study.....	55
A.4	Determination the effect of initial concentration for kinetic study was analyzed by HPLC.....	56

## LIST OF FIGURES

<b>Figure</b>		<b>Page</b>
2.1	Chemical structure of 2,4-Dichlorophenol.....	5
2.2	Electron-hole pair formation when radiated by light.....	9
2.3	Electron-hole pair recombination.....	9
2.4	Crystal structure of anatase TiO <sub>2</sub> .....	10
2.5	TiO <sub>2</sub> photocatalyst: the pollutants are oxidized and reduced into harmless products.....	12
3.1	Schematic diagram of photocatalytic reactor for photodegradation of 2,4-DCP.....	19
4.1	TG-DTA curves of Ag-TiO <sub>2</sub> sample contain PEG.....	20
4.2	SEM images reveal surface morphology of Ag-TiO <sub>2</sub> . (a) and (b) represent Ag-TiO <sub>2</sub> without PEG ,(c) and (d) represent Ag-TiO <sub>2</sub> with PEG 0.008 mol%.....	21
4.3	XRD pattern of Ag-TiO <sub>2</sub> samples compared with TiO <sub>2</sub> standard....	22
4.4	UV-DRS spectra of Ag-TiO <sub>2</sub> samples compared with TiO <sub>2</sub> standard.....	24
4.5	Plot of zeta potential of different amounts of PEG in photocatalyst suspensions.....	26
4.6	XANES spectra of Ag-TiO <sub>2</sub> samples compared with standard materials: Ti-K-edge (a) and Ag-L <sub>3</sub> -edge (b).....	27

<b>Figure</b>		<b>Page</b>
4.7	Determination of $K_2S_2O_8$ range in photodegradation of 2,4-DCP...	28
4.8	Normal probability plot of the residuals for %degradation of 2,4-DCP.....	33
4.9	Plot of predicted and actual values for %degradation of 2,4-DCP...	33
4.10	Plot of the standardized residuals versus the fitted values.....	34
4.11	Plot of the standardized residuals in the order of the corresponding observations.....	34
4.12	Main effects plot of variables by mean values of %degradation.....	35
4.13	Surface plot of the response (%removal of 2,4-DCP) versus catalyst loading and PEG content (a), catalyst loading and persulfate (b), and PEG content and persulfate (c).....	36
4.14	The photocatalytic activity of different initial concentration as a function of time.....	38
4.15	Plot of $\ln(C_0/C)$ observed as a function of time.....	38
4.16	Plot of the reciprocal of the initial rate $r_0^{-1}$ versus the reciprocal of the initial 2,4-DCP' concentration $C_0^{-1}$ for photocatalytic degradation of 2,4-DCP.....	40
4.17	Photocatalytic degradation of 2,4-DCP at different condition.....	42
A.1	Energy band gap of Ag-TiO <sub>2</sub> without PEG(a), 0.001 mol% PEG (b), 0.004 mol% PEG(c), and 0.008 mol% PEG(d).....	52
A.2	Calibration curve plot of peak area as a function of 2,4-DCP concentration.....	54



# CHAPTER I

## INTRODUCTION

### 1.1 Motivation

As numerous environmental problems become great concern, wastewater contaminated by hazardous pollutants is one of the most important problems which can cause adverse effect to human beings and aquatic life. Inefficient wastewater treatment leads to wastewater contamination by various types of organic pollutants such as chlorinated benzenes, chlorinated toluenes and chlorinated phenols or chlorophenols (Brigden, Labunska, and Stringer, 2003). Among various types of chlorophenols, 2,4-dichlorophenol (2,4-DCP) has been of great concerned. Effluents from these manufacturing industries are significant source of 2,4-DCP residuals. It is well known that chlorinated compounds are toxic because of the chlorine contained in their structure. The presence of 2,4-DCP in the environment will become a serious problem in the future, thus it is very urgent to develop an effective method to remove these contaminants to reduce or eliminate the impact of chlorophenols on the environment. Conventional treatment processes such as biological treatments are not very effective for the degradation of chlorinated phenols (Wang, H. and Wang, J., 2008). Photocatalysis has been a very promising alternative technology in contaminated wastewater treatment because of their high degradation efficiency (Gaya and Abdullah, 2008).

Titanium dioxide ( $\text{TiO}_2$ ) is a photocatalyst which is widely used for the degradation of organic contaminants because it exhibits good physical and chemical stability, high catalytic activity, and high oxidative power. Although  $\text{TiO}_2$  is good catalyst, it has limitations in visible region and high rate of electron-hole recombination (Seery et al., 2007). To overcome these limitations of  $\text{TiO}_2$  in which high recombination rate and the limit of using in visible region, various researchers studied in this aspect to improve photocatalytic efficiency of  $\text{TiO}_2$  photocatalyst for practical application. Xin et al. (2004) reported an improvement of photocatalytic activity of  $\text{TiO}_2$  by depositing noble metals such as Pt, Pd, Rh, Ag and Au. The



deposited metals on the surface of  $\text{TiO}_2$  can produce traps to capture the photoinduced electrons or holes leading to the reduction of electron-hole recombination in photocatalytic processes and increase in the visible light absorption capability. However, some noble metals such as Pt, Pd, Rh, and Au are too expensive to be used in industrial scale. Thus, the research of Ag modified  $\text{TiO}_2$  has more significant practical value for industrial application (Xin et al., 2004). Liu et al. (2004) quoted that doping with silver is most suitable for industrial applications due to its low cost and easy preparation.

Chao et al. (2003) studied on pure  $\text{TiO}_2$  and Ag doped  $\text{TiO}_2$  powders prepared by the sol-gel process. They found that Ag dopant (2-6 mol%) can increase the surface area of  $\text{TiO}_2$  powder which exhibits a great potential in improving the photocatalytic activity. Dobosz and Sobczyński (2003) found that the photodeposition of small amounts of metal silver (0.5 wt%) on the surface of  $\text{TiO}_2$  enhanced its photoactivity which leads to total phenol decomposition. Lee et al. (2005) investigated the presence of Ag in Ag- $\text{TiO}_2$  nanoparticle prepared by sol-gel method using a reduction agent which improved the photodegradation of *p*-nitrophenol and the photocatalytic activity of Ag- $\text{TiO}_2$  increased with increase in  $\text{AgNO}_3$  content. Seery et al. (2007) studied on visible absorption capacity of Ag doped  $\text{TiO}_2$  and found that increase amounts of Ag resulted in higher visible light absorption capability of the materials which significant red shifts. This leads to the conclusion that the silver samples achieve higher surface adsorption towards visible light, and hence result in better photodegradation. Moreover, Seery et al. (2007) found that the synthesis of  $\text{TiO}_2$  and Ag doped  $\text{TiO}_2$  involved the use of acetic acid and titanium isopropoxide can be prepared stable silver doped anatase material at high temperature and also provided homogeneously distribution of silver in samples after calcined at  $600^\circ\text{C}$ . During calcination, the uniformly dispersed  $\text{Ag}^+$  ions would gradually migrate from the bulk of the  $\text{TiO}_2$  to the surface by enhancing the crystallinity, resulting in metallic silver deposited on the surface on calcinations. Seery et al. (2007) also studied the degradation of model dye under visible light by silver doped titanium dioxide and found that increasing amount of silver, 5 mol% Ag- $\text{TiO}_2$ , significantly increase the rate of degradation of a model dye.

To further enhance the photocatalytic activity, the addition of polyethylene glycol (PEG) can be used to prepare the photocatalyst with high specific surface area. Bu et al. (2005) studied on TiO<sub>2</sub> porous thin films synthesized using sol-gel method with PEG as the template. The result shows higher in surface area indicated that PEG plays a templating role in the formation of the inorganic porous structure. Thus, PEG plays a very important in the evolution of the nanostructure TiO<sub>2</sub>.

In this work, the study focus on the photodegradation of 2,4-DCP in aqueous suspension by using Ag-doped TiO<sub>2</sub> photocatalyst prepared by sol-gel method in the presence of PEG under visible light irradiation.

## **1.2 Objectives**

- 1.2.1 To synthesize and characterize the physical and chemical properties of Ag-TiO<sub>2</sub> by Thermogravimatic analysis-differential thermogravimatic analysis (TG-DTA), X-ray diffraction (XRD), UV-vis diffuse reflectance spectroscopy (UV-DRS), Brunauer-Emmett-Teller (BET), scanning electron microscopy (SEM), X-ray absorption spectroscopy (XAS), and Zeta potential technique.
- 1.2.2 To study the photodegradation of 2,4-dichlorophenol (2,4-DCP) in aqueous solution under visible light irradiation by silver doped titanium dioxide (Ag-TiO<sub>2</sub>) synthesized using polyethylene glycol (PEG) as template.
- 1.2.3 To investigate the best conditions for the photodegradation of 2,4-DCP.

## **1.3 Scope of the study**

- 1.3.1 The photocatalysts are synthesized by sol-gel method.
- 1.3.2 Titanium (IV) isopropoxide is used as precursor suspended in acetic acid and doped with silver by adding AgNO<sub>3</sub> as silver source.
- 1.3.3 Ag-TiO<sub>2</sub> is added with different amount of PEG; 0, 0.001, 0.004, and 0.008 molar ratios of precursor.

- 1.3.4 Ag-TiO<sub>2</sub> is characterized by TG-DTA, XRD, UV-DRS, BET, SEM, XAS, and Zeta potential technique.
- 1.3.5 The photodegradation of 2,4-DCP is conducted under batch reactor process set up at 25°C under visible light irradiation using Xenon lamp cut off at 400 nm as light source.
- 1.3.6 The optimal amount of PEG loading in Ag-TiO<sub>2</sub>, initial concentration of 2,4-DCP, photocatalyst loading, concentration of K<sub>2</sub>S<sub>2</sub>O<sub>8</sub> and photodegradation efficiency in photodegradation of 2,4-DCP are examined.
- 1.3.7 Box-Behnken design is used as experimental design.
- 1.3.8 High performance liquid chromatography (HPLC) is used as analytical equipment for photocatalytic study.

#### 1.4 Expected Outcome

- 2,4-DCP can significantly be degraded by Ag-TiO<sub>2</sub> photocatalyst under visible light irradiation.
- Ag-TiO<sub>2</sub> photocatalyst synthesized using PEG as template would be an efficient photocatalyst in the treatment of waste water contamination by 2,4-DCP.
- Gain better understanding in the characteristic of Ag-TiO<sub>2</sub> synthesized using PEG and without PEG related to the photocatalytic degradation of 2,4-DCP



## CHAPTER II

### LITERATURE REVIEW

#### 2.1 Chlorophenols (CPs)

##### 2.1.1 General information of chlorophenols (CPs)

Chlorophenols (CPs) are a group of chemicals in which chlorines (between one and five) are added to phenol. Chlorophenols are manufactured by chlorination of phenol at high temperatures (Agency for toxic substances and disease registry (ATSDR), 1999: online). They have been widely employed in many industrial processes as synthesis intermediates or as raw materials in the manufacturing of herbicides, fungicides, pesticides, insecticides, pharmaceuticals, and dyes (Pera-Titus et al., 2004). There are five basic types of chlorophenols including monochlorophenols, dichlorophenols, trichlorophenols, tetrachlorophenols, and pentachlorophenols (ATSDR, 1999: online). Among various types of chlorophenols, 2,4-dichlorophenol (2,4-DCP) has been of great concern. 2,4-DCP is one of the 126 toxic organic compounds listed by the Environmental Protection Agency (Environmental Protection Agency (EPA), 2008: online) because of its high toxicity, nonbiodegradability, and difficulty to remove from the environment (Pera-Titus et al., 2004). Chemical structure and chemical-physical properties of 2,4-DCP are shown in Figure 2.1 and Table 2.1 (ATSDR, 1999: online) respectively.

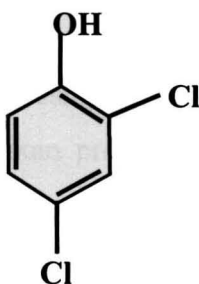


**Figure 2.1** Chemical structure of 2,4-Dichlorophenol.

**Table 2.1** Chemical and physical properties of 2,4-DCP.

<b>Properties</b>	<b>Values</b>
Chemical formula	C <sub>6</sub> H <sub>4</sub> Cl <sub>2</sub> O
Synonyms	2,4-DCP, 2,4-Dichlorohydroxybenzene
Cas number	120-83-2
Molecular weight	163
Color/ Physical state	White/Solid
Melting point	45°C
Boiling point	210°C
Density	1.383 at 60°F/25°C
Odor	Strong medical odor
Solubility	4500 ppm (in water at 25°C)
pK <sub>a</sub>	7.68

### 2.1.2 Use of 2,4-dichlorophenol (2,4-DCP)

2,4-DCP is an important chemical precursor for the production of a widely used herbicide and wood preservative (Wang, H. and Wang, J., 2008). Furthermore, it is also used in the manufacturing of industrial and agricultural products such as pesticides, germicides, soil sterilants, seed disinfectants, and antiseptics (Brigden et al., 2003: online). Effluents from these manufacturing industries are significant source of 2,4-DCP residuals.

There were some reports of 2,4-DCP contamination in Thailand. In the monitoring of endocrine disruptor compounds in the coastal hydrosphere of Thailand, 2,4-DCP was detected especially in river water samples collected from river and sea along the coastal area in the upper gulf of Thailand (Ruchaya Boonyatumanond et al., 2001: online). In another case, the investigation of environmental pollutants in the Bangpoo industrial estate, Samut-Prakan province of Thailand showed widespread contamination in and around the estate with a range of toxic and persistent organic pollutants including 2,4-DCP. The presence of organic contaminants in the treated water is a clear indication of the insufficient treatment of effluents which leads to



continuous pollution of the environment with persistent and toxic substances (Brigden et al., 2003: online).

### **2.1.3 Environmental standards for 2,4-DCP**

According to EPA's compilation of national recommended water quality criteria for the protection of aquatic life and human health in surface water, the recommended criterias for 2,4-DCP, in case of human health for the consumption of water and organism, are 70 µg/L and 290 µg/L respectively (EPA, 2008: online). The EPA recommended that for drinking water, the concentration of 2,4-DCP should not more than 0.02 mg/L. Official Journal of the European Communities in Council Directive 86/280/EEC determined 20 µg/L as the minimum quality objective of water impose for 2,4-DCP (Estevinho et al., 2007). Furthermore, the minimal risk levels (MRLs) for hazardous substances listed by ATSDR determined MRLs 0.003 mg/kg/day (oral route) for 2,4-DCP (ATSDR, 2009: online). In addition, the Department of Pollution Control (PCD) of Thailand established a standard of industrial effluents for the phenol compounds to be not more than 1 mg/L.

### **2.1.4 Environmental and health concern on 2,4-DCP**

Due to the wide utilization of 2,4-DCP, there has been concerned on effect to human health, aquatic life and animals. Because of dreadful toxicity, disturbing to human, and animal's endocrine system of 2,4-DCP has caused researchers' attention (Bao-xiu, Xiang, and Peng, 2007). There are an increasing attention in the risks of 2,4-DCP related to skin adsorption under the EPA's testing program for high production-volume chemicals. 2,4-DCP causes a number of adverse health effects not only the inhalation of dust containing 2,4-DCP irritate the respiratory tract but also the detrimental effects on kidneys, liver, and blood-forming organs (Ormad, Ovelleiro, and Kiwi, 2001). Furthermore, the report shows that 2,4-DCP is harmful toxic to aquatic life and animals due to the dichlorophenols are very toxic to the single-celled eukaryotic organism *Tetrahymena pyriformis* which is comparable in sensitiveness and responsiveness to human tissue cells (Brigden et al., 2003: online). Strong resistance to physical, chemical, and biological treatments of chlorophenols can cause

harm on living organisms including human beings. It is well known that chlorinated compounds are toxic because of the chlorine contained in their structure. The presence of 2,4-DCP in the environment will become a serious problem in the future, thus it is very urgent to develop an effective method to remove these contaminants to reduce or eliminate the impact of chlorophenols on the environment. Conventional treatment processes such as biological treatments are not very effective for the degradation of chlorinated phenols (Wang, H. and Wang, J., 2008), but 2,4-DCP can strongly inhibit activated sludge bacteria (Ren and Frymier, 2002). Recently, advanced oxidation processes (AOPs) such as UV/Ozone photolysis, UV/H<sub>2</sub>O<sub>2</sub> photolysis, Fenton/Photo-Fenton, and photocatalysis have been applied successfully in wastewater treatment contaminated by synthetic organic chemicals have attracted much attention (Wang, H. and Wang, J., 2009). Photocatalysis is one of the AOPs which focus on the degradation of various organic pollutants.

## **2.2 Basic principles of photocatalysis**

Photocatalysis is catalysis under light irradiation (Kaneko and Okra, 2002) in which light and catalyst are used together to accelerate chemical transformation. Photocatalysis is one of the AOPs, very promising alternative to conventional processes in contaminated water or wastewater treatment, because of their high degradation efficiency to oxidize organic pollutant by the generation hydroxyl radicals. The hydroxyl radicals have powerful in oxidation ability. Heterogeneous photocatalysis has proved to be of an efficient tool for degrading both aquatic and atmospheric organic contaminants. The process involves the acceleration of photoreaction in presence of semiconductor photocatalyst (Gaya and Abdullah, 2008) such as TiO<sub>2</sub>, ZnO, CeO<sub>2</sub>, and CrO<sub>2</sub> (Herrmann, 1999). It is initiated when photon with energy equal to or greater than the band gap energy ( $E_g$ ) of the photocatalyst reach the photocatalyst surface resulting to molecular excitation.  $E_g$  is the difference energy between the filled valence band (VB) and the empty conduction band (CD) of the photocatalyst. This molecular excitation results in the generation of mobile electron in the higher energy conduction band ( $E_{cb}$ ) and positive hole in the lower energy valence band ( $E_{vb}$ ) of the catalyst (Lasa, Serrano, and Salaices, 2005) as



shown in equation (2.1) and the reaction shows in Figure 2.2 (Chatterjee and Dasgupta, 2005).

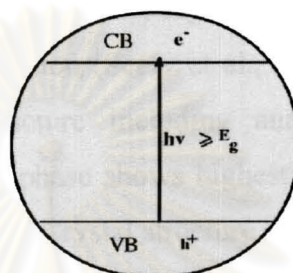
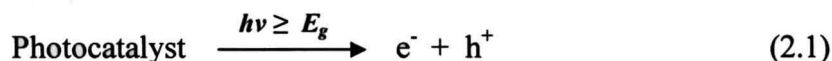


**Figure 2.2** Electron-hole pair formation when radiated by light.

The initial step in photocatalytic reaction is electron-hole pair generation which leads to the utilization of the electron-hole ( $h^+$ ) for oxidation process and eventually to capture the  $e^-$  for reduction process, as well as the formation of super oxides anion and hydrogen peroxide from oxygen (Lasa et al., 2005).

There is a competing electron and electron-hole recombination step (reverse of equation (2.1)) as shown in Figure 2.3 (Chatterjee and Dasgupta, 2005). These result in low efficiency of photocatalyst. Electron-hole recombination can be considered as the major factor limiting the efficiency of the photocatalytic reaction (Lasa et al., 2005). Many studies tried to prevent electron-hole recombination to improve the photocatalytic efficiency which enhances its application in water and air purification.

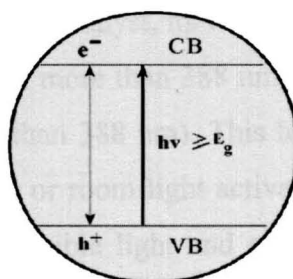


**Figure 2.3** Electron-hole pair recombination.

### 2.2.1 Titanium dioxide photocatalyst

Titanium dioxide ( $\text{TiO}_2$ ) is a semiconductor photocatalysts which is widely used in the degradation of organic contaminants in water and air.  $\text{TiO}_2$  exhibits good physical and chemical stability, high catalytic activity, high oxidative power, low cost, and ease of production (Seery et al., 2007). In general,  $\text{TiO}_2$  have three main types of crystal structure including anatase, rutile, and brookite (Fujishima, 2008).  $\text{TiO}_2$  in anatase phase shows highest photocatalytic activity than other phases (Hoffmann et al., 1995). Crystal structure of anatase shows in Figure 2.4 (Diebold, 2003).  $\text{TiO}_2$  in the anatase form appears to be the most practical of the semiconductors for widespread environmental application such as water purification, wastewater treatment, hazardous waste control, air purification, and water disinfection (Hoffmann et al., 1995).

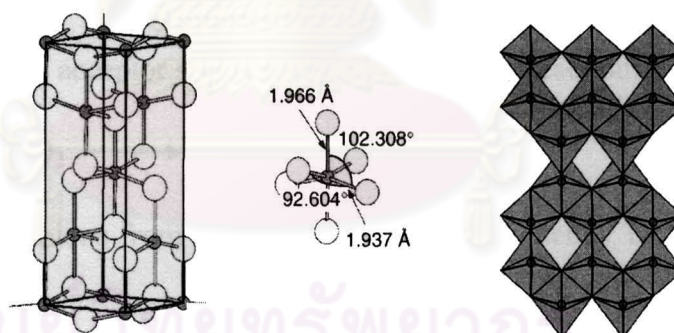
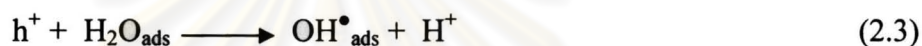


**Figure 2.4** Crystal structure of anatase  $\text{TiO}_2$ .

Although  $\text{TiO}_2$  is a good catalyst, its wide band gap (3.2 eV) limits the use in visible light region (wavelength more than 388 nm) because  $\text{TiO}_2$  is only active in UV irradiation (wavelength less than 388 nm). This has consequent implications for the use of  $\text{TiO}_2$  materials as solar or room-light activated photocatalysts, because the majority of sunlight consists of visible light and only a 3–5% of UV light. Hence increasing the efficiency of visible photocatalysis is important for the practical application of this technique in the future (Seery et al., 2007).

### 2.2.2 Photocatalytic reaction of TiO<sub>2</sub>

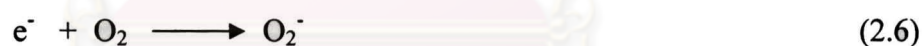
The reaction pathway of TiO<sub>2</sub>, which proposed by Lasa et al. (2005), are listed in the following equations. Firstly, TiO<sub>2</sub> photocatalyst generates an electron and electron-hole after being irradiated by UV light as described in equation (2.1). Then electron transfer from the adsorbed substrate (RX<sub>ad</sub>), adsorbed water or the OH<sub>ad</sub> ion, to the electron-hole. These reactions can be written as follows;



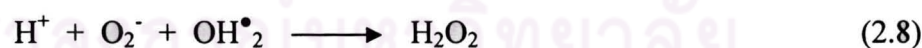
The high concentrations of OH<sup>-</sup> are given water dissociation into ions.



Oxygen acts as acceptor species in electron transfer reaction.



Super-oxide anions from equation (2.6) can subsequently be involved in the following reaction.



Photoconversion of hydrogen peroxide gives more OH<sup>•</sup> free radical groups.



Finally, OH<sup>•</sup> radical oxidized organic adsorbed pollutants (RX<sub>ad</sub>) onto the surface of the TiO<sub>2</sub> particles.





The  $\text{OH}^\bullet$  radical in equation (2.10) are very reactive and attack the pollutant molecule to degrade it into mineral acid carbon dioxide, and water. The schematic diagram of  $\text{TiO}_2$  photocatalysis shows in Figure 2.5 (Pure green coating, 2009: online).

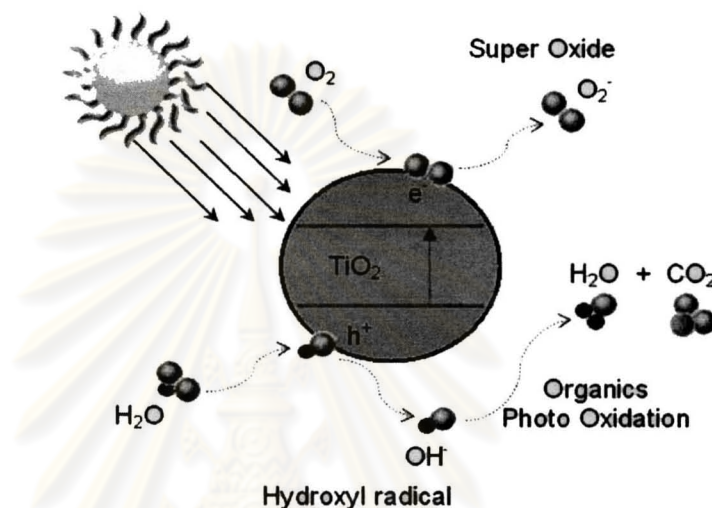


**Figure 2.5**  $\text{TiO}_2$  photocatalytic mechanism: the pollutants are oxidized and reduced into harmless products.

### 2.2.3 Photocatalyst preparation by sol-gel method

Sol-gel method is well known technique in the preparation of  $\text{TiO}_2$  photocatalyst. The sol-gel process offers unique advantages in synthesizing nanoscale  $\text{TiO}_2$  powder such as better control over stoichiometric composition, ease of synthesis, better homogeneity, and production of high purity powder (Qiu and Kalita, 2006). In a typical, sol-gel method, a colloidal suspension, or a sol, is formed from the hydrolysis and polymerization reaction of the precursor. The precursor is usually inorganic metal salts or metal organic compounds such as metal alkoxides (Chen and Mao, 2007) because alkoxide is easily purified by distillation which can produce purity  $\text{TiO}_2$  (Lasa et al., 2005). Complete polymerization and loss of solvent lead to the transition from the liquid sol into a solid gel phase (Chen and Mao, 2007). Additionally, the metal alkoxide is usually applied preparation method as precursor

such as titanium isopropoxide (Seery et al., 2007) and titanium n-butoxide (Yu et al., 2005).

#### **2.2.4 Surface modification of TiO<sub>2</sub> by metal doping**

The surface modification of TiO<sub>2</sub> photocatalyst by doping metal involves introducing metal impurity ions on the photocatalytic properties of TiO<sub>2</sub> which has been another interested area of semiconductor modification. The benefit of metal doping species is the improved trapping of electrons to inhibit electron-hole recombination during illumination. It is believed that these metals create acceptor and donor centers where direct recombination occurs (Linsebigler, 1995). Another reason for the improvement of the performance of TiO<sub>2</sub> nanomaterials is to increase their optical activity by shifting the onset of the response from the UV to the visible region (Chen and Mao, 2007).

#### **2.2.5 Addition of polyethylene glycol (PEG) as template**

Template synthesis method has been playing an important role in the fabrication of nanocrystalline oxides with various surface and crystalline properties. Especially, polymers have been acknowledged as crucial template for the preparation of materials with novel properties and morphologies (Huh et al., 2003: cited in Jiao et al., 2008). The polymer templates can exhibit very complex phase behavior in an aqueous solution and have been expected to form new products with varied structure, together with improving the properties of known materials (Jikei et al., 2007: cited in Jiao et al., 2008). Among all the used polymer templates, polyethylene glycol (PEG) is very popular, and it has been reported that it could lead to the formation of nanocrystals with high performance. PEG has excellent water solubility, biocompatible lubricity, thermal stability plus its features of non-toxic, non-irritating, and moisturizing. The important role of PEG in the synthesis of TiO<sub>2</sub> in the presence of PEG as template has been widely reported. Bu et al. (2005) studied on TiO<sub>2</sub> porous thin films synthesized in such a sol-gel method using PEG as a template. The result showed higher in surface area indicated that PEG plays a templating role in the formation of the inorganic porous structure. Arconada et al. (2009) prepared porous

TiO<sub>2</sub>-anatase films by sol-gel method with and without PEG. The result showed that maximum surface area was obtained for coatings prepared from TiO<sub>2</sub> sol with PEG. Yu et al. (2005) reported the synthesis of ultrafine nanocrystalline anatase powders were achieved by the hydrothermal method from titanium n-butoxide in the presence of PEG. Titanium nanocrystals with exclusive anatase crystal structure have been successfully prepared. Yu and co-workers suggested that PEG enhanced the homogenous of the metal cations. Since PEG has ether oxygen in its chain, it can interact with metal ions. The interaction and random arrangement of the polymer chain make the metal cations mixed at the molecular level. Moreover, Zhang et al. (2003) reported that PEG was also used as a structure-directing agent for organizing the network-forming metal-oxide species.



ศูนย์วิทยทรัพยากร  
จุฬาลงกรณ์มหาวิทยาลัย



# CHAPTER III

## MATERIALS AND METHODS

### 3.1 Materials

All the materials in this study were analytical reagent grade with no further purification.

- Titanium (IV) isopropoxide (TTIP) (98<sup>+</sup>%, Acros)
- Acetic acid glacial (Carlo)
- Silver nitrate (AgNO<sub>3</sub>) (Carlo)
- Polyethylene glycol (PEG) (molecular weight average 20,000) (Merk)
- 2,4-Dichlorophenol (99%, Acros)
- Sodium nitrite
- Dipotassium peroxodisulfate (K<sub>2</sub>S<sub>2</sub>O<sub>8</sub>) (Carlo)
- Methanol, HPLC grade (Lab scan)
- Water, HPLC grade (Lab scan)

### 3.2 Photocatalyst preparation

Ag-TiO<sub>2</sub> was prepared by sol-gel method. Firstly, TTIP was added into acetic acid. Distilled water, mixed with PEG and the desire amount of AgNO<sub>3</sub>, was dropped into the mixture of TTIP and acetic acid with vigorous stirring. The ratios of mixture solution of TTIP, acetic acid, and deionised water were 1:10:100 molar ratios and adding with different amount of PEG; 0, 0.001, 0.004, and 0.008 molar ratios of precursor. After that, all of the mixture solution in each sample was stirred at 5°C for 12 hours. Next, the solution was dried in water bath at 80°C until all the solution was completely dried. Finally, the dried material was calcined at 600°C by setting ramp rate at 5°C/min. for 2 hours.

### 3.3 Photocatalyst characterization

In this study, the following techniques were applied to determine the chemical and physical properties of the photocatalyst.

#### 3.3.1 Thermogravimetric-differential thermogravimetric analysis (TG-DTA)

TG-DTA was employed to determine a material's thermal stability and its fraction of volatile components by monitoring the weight change regarding to temperature program. Certain amount of materials was placed in a platinum crucible and the condition using a constant heating rate of 10°C/min from 30°C (room temperature) to 800°C under air atmosphere.

#### 3.3.2 X-ray diffraction (XRD)

To determine the crystal structure, crystallinity, and estimate crystallite size of photocatalyst, a Bruker AXS powder X-ray diffractometer with Cu K $\alpha$  radiation source ( $\lambda=1.5406\text{\AA}$ ) at 40 kV, 40 mA was employed. The XRD patterns were recorded in the  $2\theta$  angle range of 20-80° with a step size of 0.02° and a time step of 2.0 sec to assess the structure of the matrix. The average crystallite size of all samples was calculated using Scherrer equation as shown in equation (3.1).

$$D = \frac{K\lambda}{\beta \cos \theta} \quad (3.1)$$

Where D is the crystallite size, K is a constant usually taken 0.9,  $\lambda$  is the wavelength corresponding to the Cu K $\alpha$  radiation,  $\beta$  is the full width at half maximum (FWHM) of the diffraction peak of anatase (101), and  $\theta$  is the diffraction angle.

#### 3.3.3 UV-vis diffuse reflectance spectroscopy (UV-DRS)

UV-DRS technique is used to record absorbance capacity of the powder. UV-DRS spectra of samples were recorded on HITACHI U-3501 UV-vis

spectrophotometer with an integrating sphere attachment to determine absorbance of the photocatalysts. The scanning range was between 300 and 800 nm and the pure powder BaSO<sub>4</sub> was used as a reference.

### **3.3.4 Brunauer-Emmett-Teller (BET) method**

BET method was utilized to measure the surface area of materials. The surface area was obtained by the adsorbate, N<sub>2</sub>, at -196°C on a Micromeritics ASAP 2010 sorption analyzer where nitrogen adsorption and desorption isotherms were measured.

### **3.3.5 Scanning electron microscopy (SEM)**

Surface morphology of photocatalyst was observed SEM images by using JEOL apparatus model JSM-640 scanning microscope equipped with Sony video graphic printer (UP-897 MD).

### **3.3.6 X-ray absorption spectroscopy (XAS)**

In this study, XANES technique was used to verify the oxidation state of the particles. XANES technique was performed at beamline 8, Synchrotron Light Research Institute (Public organization) at Nakorn Rachasiman, Thailand. To set the experiment, samples were pressed into a frame covered by polyimide tape and mounted onto the sample holder. A double Ge (220) crystal monochromator was employed for selection of photon energy. The data were obtained at room temperature in fluorescent mode (Lytle). The photon energy was scanned from -30 eV below the edge to 80 eV above the edge with scan step 0.2 eV. The XANES spectra were analyzed using the conventional procedure by using Athena program. After background correction, the XANES spectra were normalized by the edge height and compared with standard references. Standard materials are Ag foil and TiO<sub>2</sub> (P25).

### **3.3.7 Zeta potential technique**

Electrokinetic interactions at the interface between aqueous electrolyte and material surfaces were identified by Zeta-meter system 3.0+ (Meditop Co., Ltd.).



### 3.4 Photocatalytic study

In this work, Box-Behnken design is used as experimental design for optimizing operating condition. The observation parameter are amount of PEG contain in photocatalyst, photocatalyst loading, and concentration of  $K_2S_2O_8$ . The range of  $K_2S_2O_8$  was determined by the photocatalytic degradation of 2,4-DCP at certain condition. The optimizing condition obtained from Box-Behnken design then used to study the effect of initial concentration of 2,4-DCP.

The experiment was conducted under batch reactor process. The photocatalytic reactor shows in Figure 3.1. The Xenon lamp cut off at 400 nm by sodium nitrite solution was used as visible light source which light intensity was approximately  $640 \text{ W/m}^2$ . The condition for observation of photocatalytic activity was holds at  $25^\circ\text{C}$  by cooling system. The pH condition in each different photocatalyst was adjusted at point of zero charge following the Zeta potential results. All samples were collected in a certain period of time with desire volume and then the solution was filtered by PTFE syringe filter  $0.45 \mu\text{m}$ . The samples were collected follow the sequence obtained from design of experiment. Photodegradation efficiency (X) is examined by the following equation (Daneshvar et al., 2003).

$$X = \left( \frac{C_0 - C}{C_0} \right) \times 100 \% \quad (3.2)$$

Where  $C_0$  = Initial concentration of 2,4-DCP.

$C$  = Concentration of 2,4-DCP at time  $t$ .

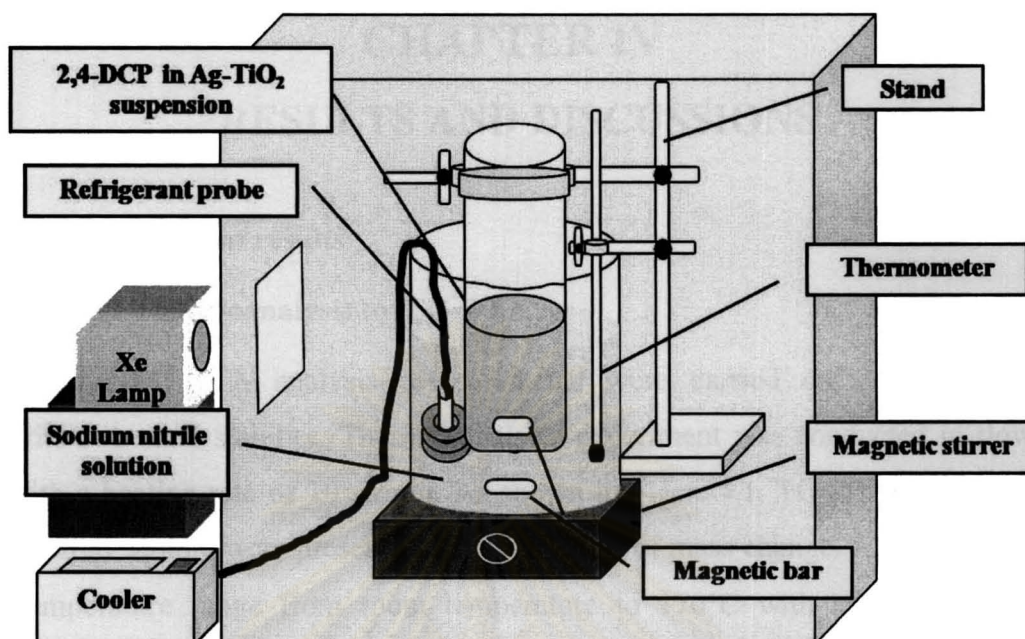


**Figure 3.1** Schematic diagram of photocatalytic reactor for photodegradation of 2,4-DCP.

### 3.5 Analytical method

In this study, high performance liquid chromatography (HPLC) (Hewlett Packard HP-Agilent 1100 series) was applied to determine the concentration of 2,4-DCP in different Ag-TiO<sub>2</sub> samples. The instrument was equipped with a UV-visible photodiode array detector set at 280 nm and configured with an Acclaim Hypercy 48-3 $\mu$ m (ID)-2.1mm (length) column. The analysis was conducted isothermally with the oven temperature set at 40°C and with an eluent (methanol-water mixture (60:40)) flow rate set at 0.1 ml/min.

# CHAPTER IV

## RESULTS AND DISCUSSIONS

### 4.1 Characterization results

#### 4.1.1 Thermoanalysis by TG-DTA

The TG-DTA analysis measurements were carried out to determine a material's thermal stability. Thermal analysis experiment was conducted in flowing air with a heating rate of 10°C/min. As shown in Figure 4.1, TG-DTA curves of as-synthesized sample were presented two main steps of mass change. At the beginning, the temperature range from room temperature to 170°C with approximately 5% weight loss could be due to the loss of water and acetic acid. Secondly, there was a large exothermic peak in the region of 300-600°C should be due to the decomposition of the organic template such as PEG including the decompose of nitrate and partly residual organics. As can be seen the large exothermic peak at 300-600°C, it could be attributed to the completely decompose of the residual organics can happened above 600°C. TG-DTA result can be revealed that calcinations temperature of Ag-TiO<sub>2</sub> samples at 600°C was obtained the completely decompose of organic compound.

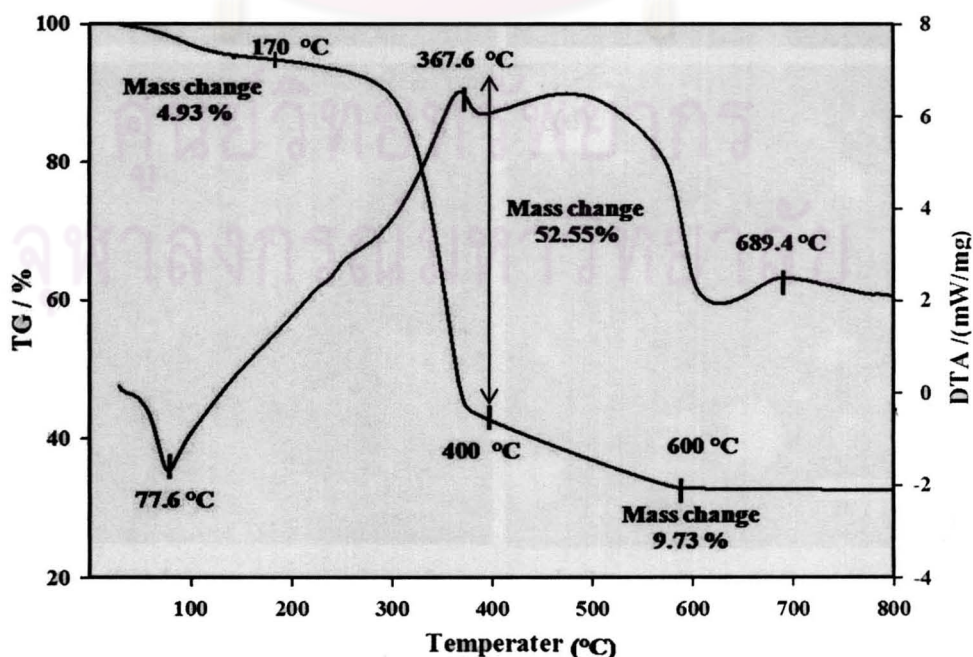
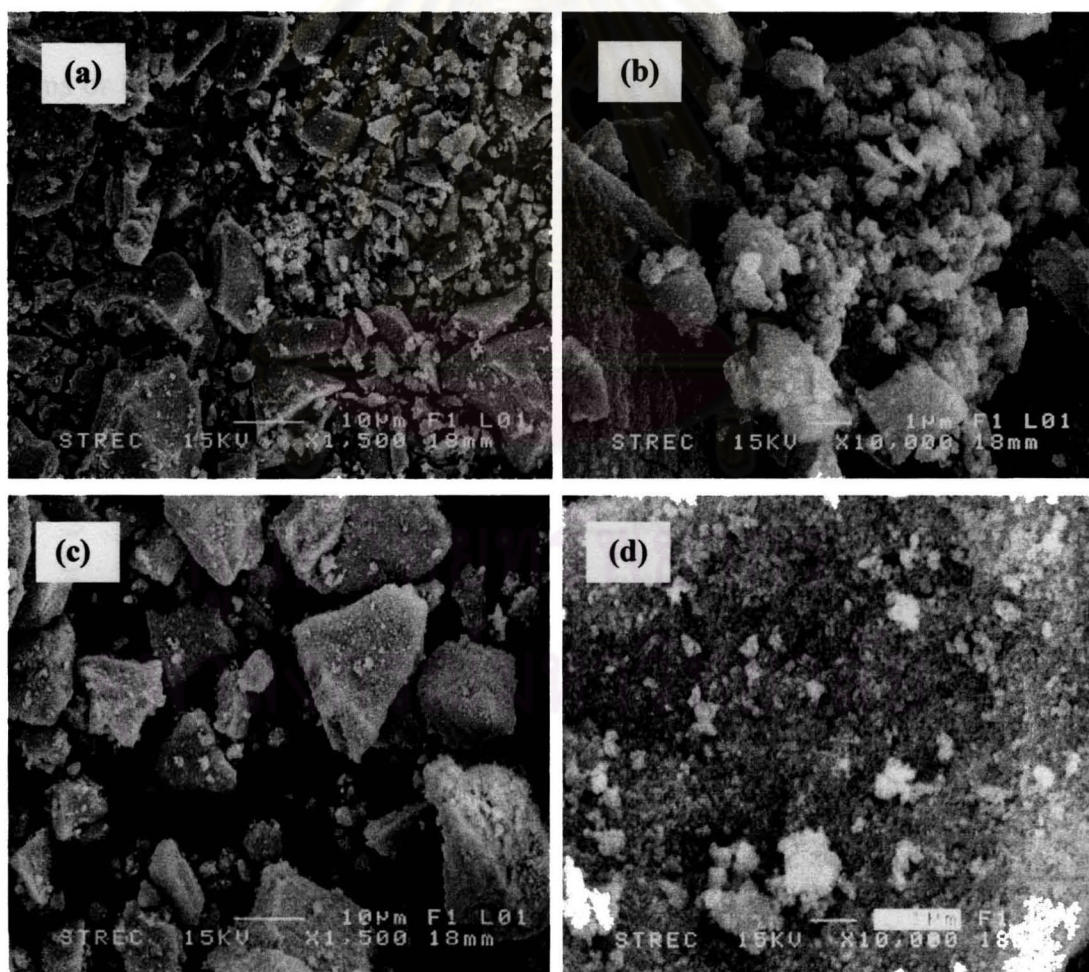


Figure 4.1 TG-DTA curves of Ag-TiO<sub>2</sub> sample contain PEG.



#### 4.1.2 Surface morphology of photocatalysts by SEM

SEM technique was performed to observe surface morphology of the Ag-TiO<sub>2</sub> both Ag-TiO<sub>2</sub> samples with PEG (0.008 mol%) and without PEG as shown in Figure 4.2. The SEM pictures of two different PEG contents revealed that there were several sizes and not specific shapes of particles in both of the two samples. It was found that the particle size ranged from around 0.1 μm to 25 μm and there were no significant differences in surface morphology. To observe the difference between the samples with PEG and without PEG content would be concerned with the average crystallite size from XRD pattern results, UV-DRS results, and BET surface area results.



**Figure 4.2** SEM images reveal surface morphology of Ag-TiO<sub>2</sub> where (a) and (b) represent Ag-TiO<sub>2</sub> without PEG, (c) and (d) represent Ag-TiO<sub>2</sub> with PEG 0.008 mol%.

#### 4.1.3 Determination of crystallite size of photocatalysts by XRD

The XRD patterns of Ag-TiO<sub>2</sub> samples show in Figure 4.3. The results obtained from XRD patterns were revealed the average crystallite size of anatase (101) phase calculated follow Scherrer equation. Crystallite size of each samples were ranged from 22-25 nm along with increasing of PEG contents; 0, 0.001, 0.004, and 0.008 mole% as shown in Table 4.1. It was noted that as increase in PEG content achieved in higher crystallite size. As can be seen from XRD patterns, each sample revealed the characteristic of Ag doped TiO<sub>2</sub> mainly in anatase phase when compared with commercial TiO<sub>2</sub> (P25). However, there was no obvious peak of Ag in samples because it probably well dispersed on TiO<sub>2</sub> surface and confined inside framework of the titania matrix (Seery et al., 2007) and metal sites were expected to be low the visibility limit of X-ray analysis (Sakthivel et al., 2004). This result suggests that their forms or locations of metal dopants could not be determined by XRD. The presence of silver particles could be identified by XANES technique.

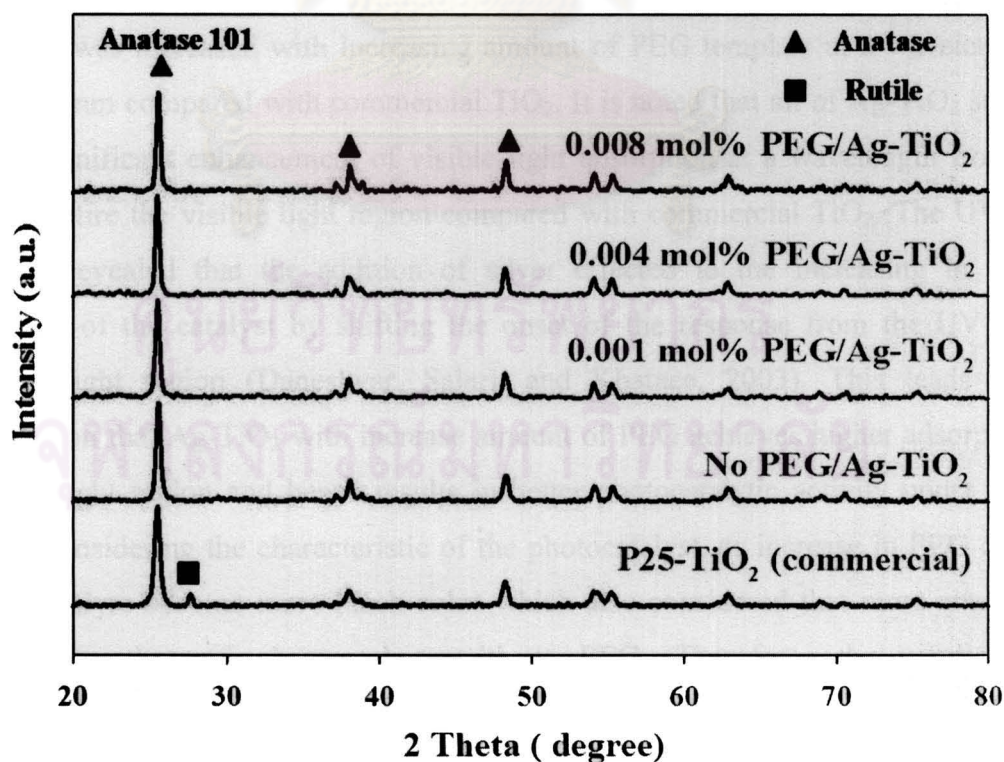


Figure 4.3 XRD pattern of Ag-TiO<sub>2</sub> samples compared with TiO<sub>2</sub> standard.



**Table 4.1** Average crystallite size of samples.

<b>Samples</b>	<b>Crystallite Size (Anatase) (nm)</b>
No PEG Ag-TiO <sub>2</sub>	22.424
0.001mol%PEG Ag-TiO <sub>2</sub>	23.527
0.004mol%PEG Ag-TiO <sub>2</sub>	24.416
0.008mol%PEG Ag-TiO <sub>2</sub>	25.581

As can be seen in Table 4.1, it was observed that crystallite sizes slightly increase as increasing in PEG content. Since the smaller size of crystallite was expected that is significant influence to photocatalytic activity because of increase in active surface area of the smaller size of catalyst particles.

#### **4.1.4 Determination visible light adsorption capacity by UV-DRS**

The UV-DRS spectra show in Figure 4.4. The adsorption capacity of calcined samples was increased with increasing amount of PEG template at a wavelength of 400-700 nm compared with commercial TiO<sub>2</sub>. It is noted that all of Ag-TiO<sub>2</sub> samples show significant enhancement of visible light absorption at a wavelength from 400 nm to entire the visible light region compared with commercial TiO<sub>2</sub>. The UV-DRS spectra revealed that the addition of silver effected to the increasing in optical property of the catalyst by shifting the onset of the response from the UV to the visible light region (Daneshvar, Salari, and Khataee, 2003). This leads to the conclusion that Ag-TiO<sub>2</sub> with increase amount of PEG achieves higher adsorption in visible light region and hence results in better photocatalytic activity under visible light. Considering the characteristic of the photocatalyst, as increase in PEG content photocatalyst become more black color which also considered that more absorb the light than that of photocatalyst without PEG. Therefore, the results from photocatalytic study probably not increase in photocatalytic activity corresponding to the UV-DRS spectra. In addition, the energy band gap ( $E_g$ ) of each sample was determined by Kubelka-Munk model. The absorption coefficient was derived from



measurements of the diffuse reflectance of the samples. For crystalline solids,  $E_g$  can be approximated as in equation (4.1).

$$kh\nu = A(h\nu - E_g)^2 \quad (4.1)$$

Where the absorption coefficient  $k$  on the frequency  $\nu$  and  $A$  is a constant. The band gap ( $E_g$ ) can be obtained by extrapolating to zero a linear fit to a plot of  $(kh\nu)^{1/2}$  against  $h\nu$  (photon energy (eV)) which is often referred to as a Tauc plot (Murphy, 2007). Tauc plot of each sample was shown in appendix.

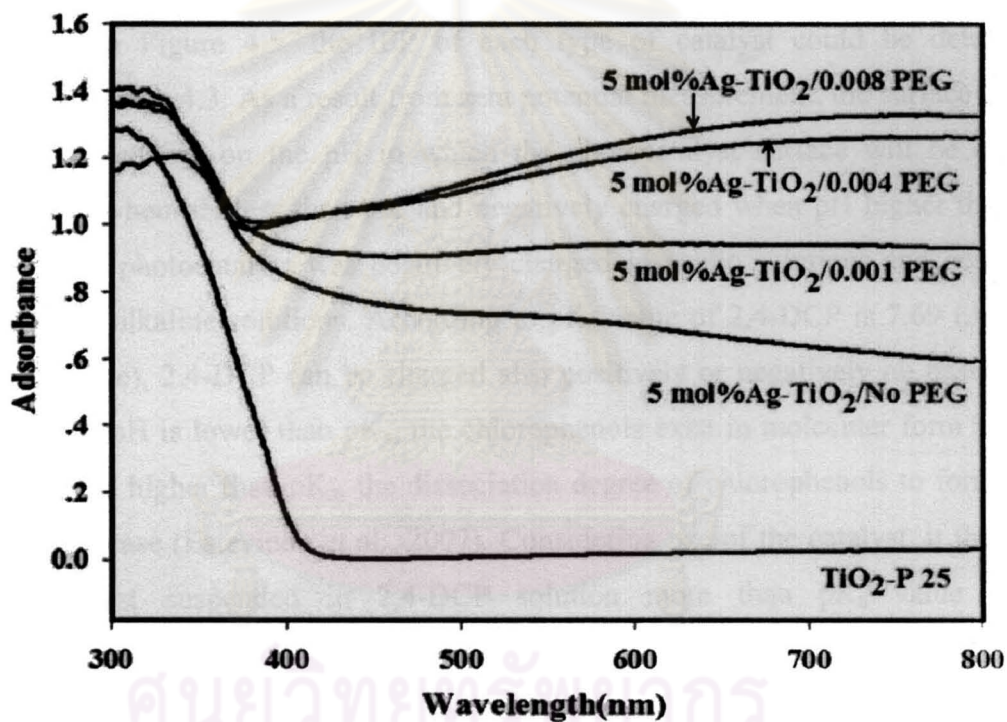


Figure 4.4 UV-DRS spectra of Ag-TiO<sub>2</sub> samples compared with TiO<sub>2</sub> standard.

Table 4.2 Energy band gap of Ag-TiO<sub>2</sub> samples.

Samples	Energy band gap ( $E_g$ )
No PEG Ag-TiO <sub>2</sub>	2.46
0.001mol%PEG Ag-TiO <sub>2</sub>	2.63
0.004mol%PEG Ag-TiO <sub>2</sub>	2.74
0.008mol%PEG Ag-TiO <sub>2</sub>	2.83

Energy band gap of each sample are shown in Table 4.2. It was found that as increasing in PEG content energy band gap was increased. The photocatalyst without PEG was the narrowest  $E_g$  which possibly was the best performance in photocatalytic activity due to it used less energy than others to excite the electron from valence band to conduction band to perform photocatalytic reaction.

#### 4.1.5 Zeta potential technique

Zeta potential measurement was used to identify surface charge by isoelectric point (IEP). This was verified by the point of zero charge (pzc) of photocatalyst. As observed in Figure 4.5, the IEP of each type of catalyst could be determined following Table 4.3. As a result from zeta potential measurement, the surface of each sample depending on the pH in which the photocatalyst surface will be charged positively when pH less than pzc and negatively charged when pH higher than pzc. Hence, the photocatalyst was positively charged in acidic solutions and negatively charged in alkaline solutions. According to  $pK_a$  value of 2,4-DCP is 7.69 (ATSDR, 1999: online), 2,4-DCP can be charged also positively or negatively on basis of the pH. When pH is lower than  $pK_a$ , the chlorophenols exist in molecular form whereas when pH is higher than  $pK_a$ , the dissociation degree of chlorophenols to form anion would increase (Estevinho et al., 2007). Considering pzc of the catalyst, if the pH of photocatalyst suspended in 2,4-DCP solution more than  $pK_a$  value of the chlorophenol (anion form), the surface of catalyst would be negatively charged resulting in a repulsion between two compounds. Therefore, if the pH condition provides at lower than  $pK_a$  of the chlorophenol (un-ionized form), the chlorophenol would be more likely to absorb on photocatalyst at pzc of photocatalyst. Hence, the condition for photocatalytic study was provided at the pzc of photocatalyst.

**Table 4.3** Zeta potential values of different PEG content in photocatalyst suspension.

Samples	Point of zero charge
No PEG Ag-TiO <sub>2</sub>	3.75
0.001mol%PEG Ag-TiO <sub>2</sub>	3.5
0.004mol%PEG Ag-TiO <sub>2</sub>	3.6
0.008mol%PEG Ag-TiO <sub>2</sub>	3.47

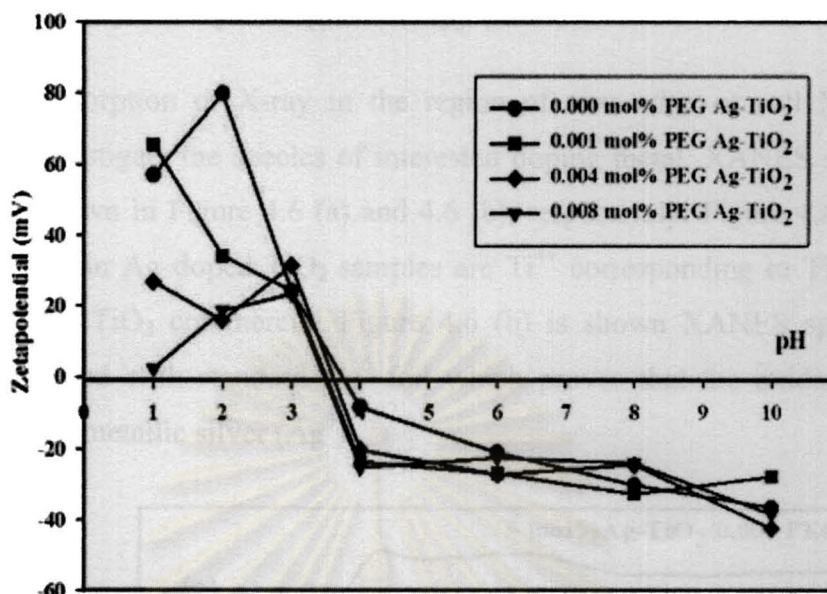


**Figure 4.5** Plot of zeta potential of different amounts of PEG in photocatalyst suspensions.

#### 4.1.6 Determination specific surface area by BET method

The results of BET surface area are presented in Table 4.4. It was noted that increasing in amount of PEG resulted in higher surface area range from about 9 to 14 m<sup>2</sup>/g. Higher surface area could be due to PEG plays a templating role in the formation of the inorganic porous structure (Bu et al., 2005). These results presented that there were no significant difference in varied amount of PEG in each photocatalyst. The Ag-TiO<sub>2</sub> with 0, 0.004, and 0.008 mol% of PEG were further used for photocatalytic study.

**Table 4.4** BET surface area of each Ag-TiO<sub>2</sub> samples.

Samples	BET surface area (m <sup>2</sup> /g)
No PEG Ag-TiO <sub>2</sub>	9.95
0.001mol%PEG Ag-TiO <sub>2</sub>	10.99
0.004mol%PEG Ag-TiO <sub>2</sub>	12.03
0.008mol%PEG Ag-TiO <sub>2</sub>	14.11



#### 4.1.7 X-ray absorption spectroscopy (XAS)

The adsorption of X-ray in the region of near edge or call XANES was selected to investigate the species of interested doping metal. XANES spectra of Ti and Ag are shown in Figure 4.6 (a) and 4.6 (b), respectively. Figure 4.6 (a) verifies that Ti species in Ag doped  $\text{TiO}_2$  samples are  $\text{Ti}^{4+}$  corresponding to  $\text{TiO}_2$  structure compared with  $\text{TiO}_2$  commercial. Figure 4.6 (b) is shown XANES spectra of Ag species compared with standard  $\text{Ag}^0$  foil which proves that the oxidation state of silver dopant is metallic silver ( $\text{Ag}^0$ ).

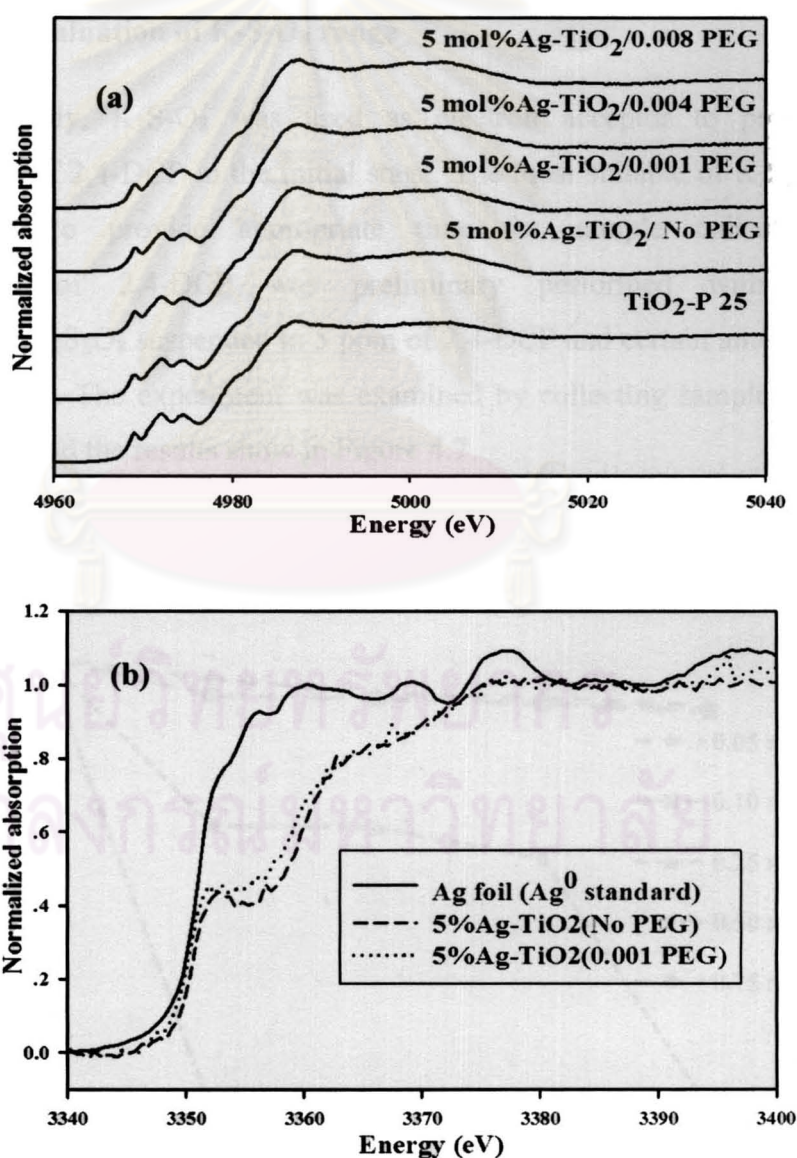


**Figure 4.6** XANES spectra of Ag-TiO<sub>2</sub> samples compared with standard materials: Ti-K-edge (a) and Ag-L<sub>3</sub>-edge (b).

## 4.2 Photocatalytic study

In order to evaluate the factor affecting to photocatalytic degradation of 2,4-DCP, the response surface methodology (RSM) based on design of experiments (DOEs) was selected to design experiment. In this work, Box-Behnken design was applied to evaluate the optimal condition in the photocatalytic study. The factor of PEG content, photocatalyst loading, and concentration of  $K_2S_2O_8$  were taken into consideration for the experimental design. In order to specify suitable range of  $K_2S_2O_8$ , the determination of  $K_2S_2O_8$  range was examined.

### 4.2.1 Determination of $K_2S_2O_8$ range

In this study,  $K_2S_2O_8$  was used as electron acceptor to promote the photodegradation of 2,4-DCP in the initial stage. The most suitable of  $K_2S_2O_8$  range was determined to provide appropriate time for sample collection. The photodegradation of 2,4-DCP was preliminary performed with different concentrations of  $K_2S_2O_8$  suspended in 5 ppm of 2,4-DCP and certain amount of  $Ag-TiO_2$  photocatalyst. The experiment was examined by collecting samples every 15 minute for 1 hour and the results show in Figure 4.7.

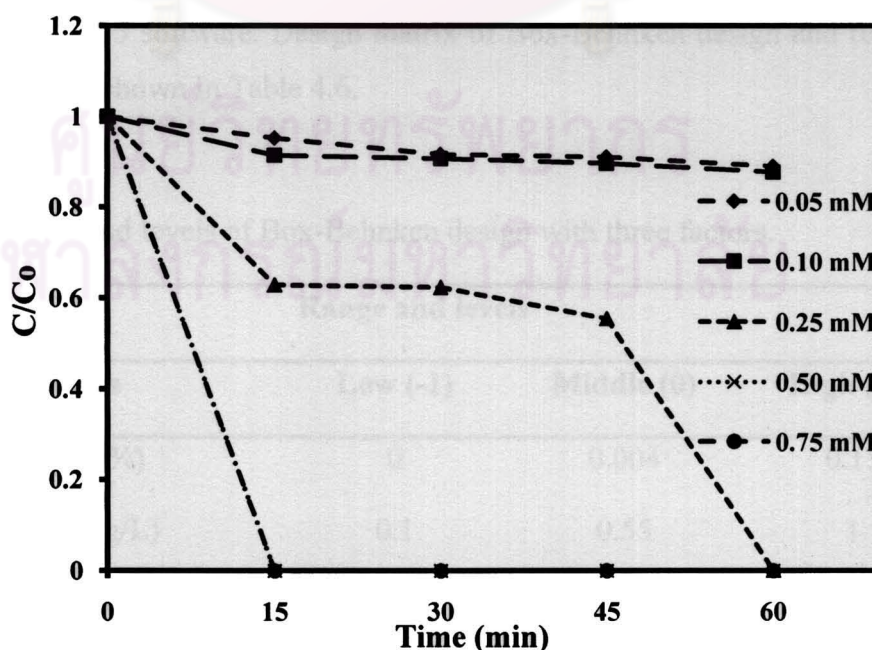


Figure 4.7 Determination of  $K_2S_2O_8$  range in photodegradation of 2,4-DCP.

From the results, it was observed that 2,4-DCP was slightly removed at 0.05 and 0.1 mM of  $K_2S_2O_8$  added. In case of 0.25 mM  $K_2S_2O_8$  added, 2,4-DCP was completely removed within 60 minutes. For 0.5 and 0.75 mM of  $K_2S_2O_8$  added, 2,4-DCP was 100% removed in 15 minutes. In order to collect sample in each batch from experimental design in 1 hour, 2,4-DCP should not reach 100% removed. According to this result, the experiment was supposed to provide the concentration of  $K_2S_2O_8$  less than 0.25 mM. Therefore, this range of  $K_2S_2O_8$  concentration at 0.05 mM (0.0014g/100 ml), 0.1 mM (0.0027g/100 ml), and 0.15 mM (0.0041g/100 ml) were varied in the study of photodegradation of 2,4-DCP by Box-Behnken design.

#### 4.2.2 Factor evaluation on 2,4-DCP photodegradation by Box-Behnken design

A three factors three levels Box-Behnken design was applied to determine the operating condition for maximizing 2,4-DCP photodegradation. The design matrix by using this design was shown fifteen trials experiment with factors of highest confidence levels. They are prescribed into three levels coded -1, 0 and 1 for low, middle and high values respectively as seen in Table 4.5. The responses were selected as the %degradation of 2,4-DCP after 1 hour of irradiation and analyzed statistically by using Minitab 15 software. Design matrix of Box-Behnken design and responses of the reaction are shown in Table 4.6.

**Table 4.5** Range and levels of Box-Behnken design with three factors.

Range and levels			
Factors	Low (-1)	Middle (0)	High (+1)
PEG content (mol%)	0	0.004	0.15
Catalyst loading (g/L)	0.1	0.55	1
$K_2S_2O_8$ concentration (mM)	0.05	0.1	0.15



**Table 4.6** Design matrix and results of Box-Behnken design.

<b>Design matrix</b>				
<b>Run Order</b>	<b>PEG content (mol %) = <math>X_1</math></b>	<b>Catalyst loading (g/L) = <math>X_2</math></b>	<b><math>K_2S_2O_8</math> (mM) = <math>X_3</math></b>	<b>Response (%Degradation)</b>
1	0.004	0.1	0.15	5.3913
2	0.008	0.1	0.1	2.7869
3	0	0.55	0.15	58.11
4	0.004	0.1	0.05	5.8824
5	0.004	0.55	0.1	33.858
6	0	0.1	0.1	7.9699
7	0.004	1	0.05	18.731
8	0.008	0.55	0.05	9.8485
9	0.008	0.55	0.15	76.3
10	0.004	1	0.15	88.235
11	0.004	0.55	0.1	38.831
12	0.004	0.55	0.1	46.201
13	0.008	1	0.1	19.424
14	0	1	0.1	60.923
15	0	0.55	0.05	17.739

A full quadratic model was evaluated for the response function base on apparent photodegradation of 2,4-DCP experimental data. The analysis was done by Minitab 15 software. The coefficients of the quadratic model, which describes %removal of 2,4-DCP (response) as a function of reaction condition (independent

variable), were calculated by a multiple regression analysis on the experimental data. The coefficients were analyzed using the analysis of variance (ANOVA) to evaluate if a given term has a significant effect ( $P \leq 0.05$ ). The adequacy of the final model was verified by graphical and numerical analysis using the Minitab 15 statistical software.

The apparent %degradation was considered as the response variable and the computed values at different factor-level combinations were treated statistically to develop the response surface model (Ray et al., 2009). A quadratic model illustrated by regression equation (equation (4.2)) was evaluated for the experimental response.

$$Y = \beta_0 + \beta_1 X_1 + \beta_2 X_2 + \beta_3 X_3 + \beta_{12} X_1 X_2 + \beta_{13} X_1 X_3 + \beta_{23} X_2 X_3 + \beta_{11} X_1^2 + \beta_{22} X_2^2 + \beta_{33} X_3^2 \quad (4.2)$$

Where Y is the predicted response,  $\beta_0$  is the model constant,  $X_1$ ,  $X_2$  and  $X_3$  are independent variables,  $\beta_1$ ,  $\beta_2$  and  $\beta_3$  are linear coefficients,  $\beta_{12}$ ,  $\beta_{13}$  and  $\beta_{23}$  are cross product coefficients and  $\beta_{11}$ ,  $\beta_{22}$  and  $\beta_{33}$  are the quadratic coefficients

For photocatalytic reaction data,  $R^2 = 93.04\%$  of the variation in yield is explained by model and the adjusted  $R^2$  is  $80.52\%$ . As seen in Table 4.7, the photocatalytic reaction data can put in the regression equation as illustrated in equation (4.3).

$$Y = 39.63 - 4.548 [\text{PEG content}] + 20.66[\text{Catalyst loading}] + 21.979[\text{K}_2\text{S}_2\text{O}_8] - 9.0791[\text{PEG content} * \text{Catalyst loading}] + 6.5201[\text{PEG content} * \text{K}_2\text{S}_2\text{O}_8] + 17.4988[\text{Catalyst loading} * \text{K}_2\text{S}_2\text{O}_8] - 2.9572[\text{PEG content}]^2 - 13.8967 [\text{Catalyst loading}]^2 + 3.8269[\text{K}_2\text{S}_2\text{O}_8]^2 \quad (4.3)$$

**Table 4.7** Estimated regression coefficients for %removal of 2,4-DCP.

Term	Coef.	Std error Coef.	T values	P values	Remark	
Constant ( $\beta_0$ )	39.63	7.056	5.616	0.002		
$X_1$	$\beta_1$	-4.548	4.321	-1.053	0.341	Not significant
$X_2$	$\beta_2$	20.66	4.321	4.781	0.005	Significant
$X_3$	$\beta_3$	21.979	4.321	5.087	0.004	Significant
$X_1 X_1$	$\beta_{11}$	-2.9572	6.360	-0.465	0.662	Not significant
$X_2 X_2$	$\beta_{22}$	-13.8967	6.360	-2.185	0.081	Not significant
$X_3 X_3$	$\beta_{33}$	3.8269	6.360	0.602	0.574	Not significant
$X_1 X_2$	$\beta_{12}$	-9.0791	6.111	-1.486	0.179	Not significant
$X_1 X_3$	$\beta_{13}$	6.5201	6.111	1.067	0.335	Not significant
$X_2 X_3$	$\beta_{23}$	17.4988	6.111	2.864	0.035	Significant

P-value is used to determine which of the effects in the model are statistically significant. According P-value less than or equal to 0.05, it represented that the factor is significant to the operating condition. Considering linear effect ( $X_1$ ,  $X_2$ ,  $X_3$ ), the factor influenced to the %degradation of 2,4-DCP were catalyst loading and concentration of  $K_2S_2O_8$  with P-value 0.005 and 0.004 respectively except the effect of PEG content had not significant factor with P-value equal to 0.341. For squared effects ( $X_1X_1$ ,  $X_2X_2$ ,  $X_3X_3$ ), there were no significant quadratic effects which meant  $X_1$ ,  $X_2$ ,  $X_3$  and %removal of 2,4-DCP in a straight line rather than curved line. For interaction effect ( $X_2X_3$ ) with P-value 0.035, it was a significant interaction effect. The effect of %degradation of 2,4-DCP, therefore, depended on the catalyst dose and concentration of  $K_2S_2O_8$ .



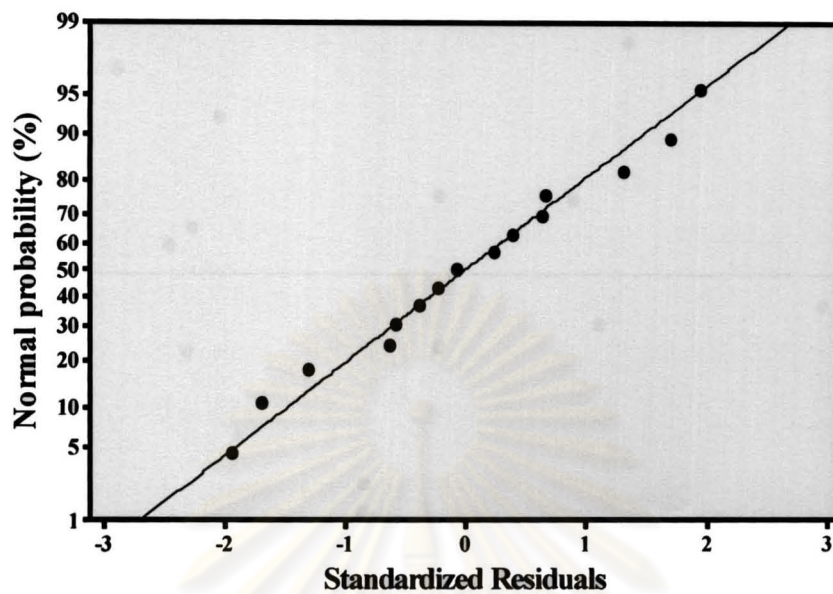


**Figure 4.8** Normal probability plot of the residuals for %degradation of 2,4-DCP.

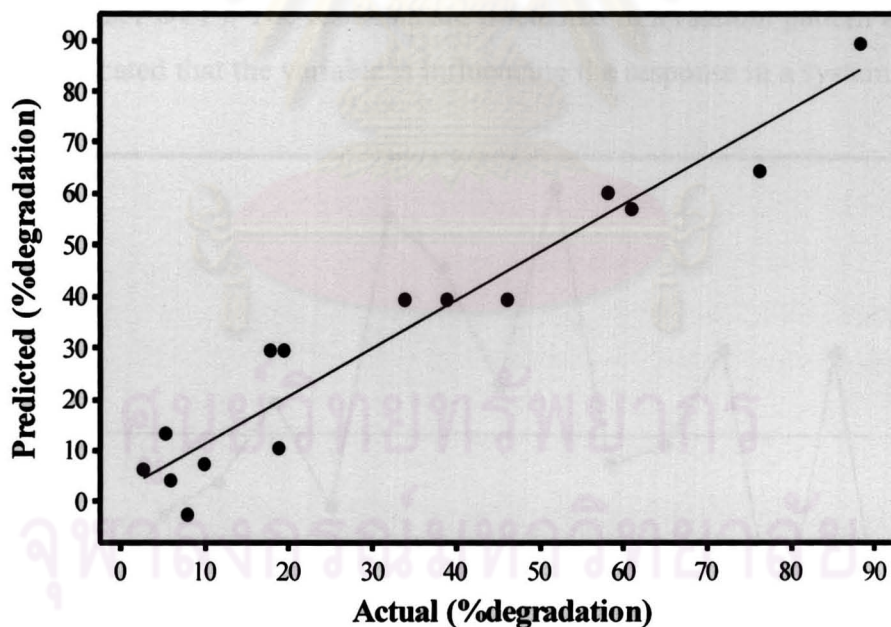


**Figure 4.9** Plot of predicted and actual values for %degradation of 2,4-DCP.

Figure 4.8 displays the residuals which are inclined on a straight line indicated that the data are fairly normal. In addition, each observed value is compared with the predicted values which are shown the regression model is practically well fitted with the observed values as seen in Figure 4.9.

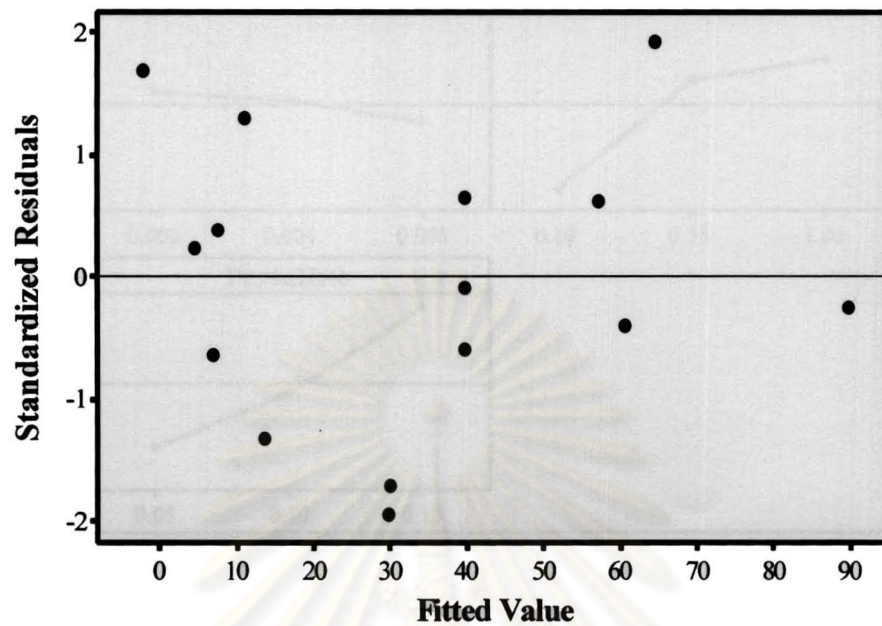


**Figure 4.10** Plot of the standardized residuals versus the fitted values (response is % degradation of 2,4-DCP). The residuals are fluctuated in a random pattern around the center line indicated that the variable is influencing the response in a systematic way.

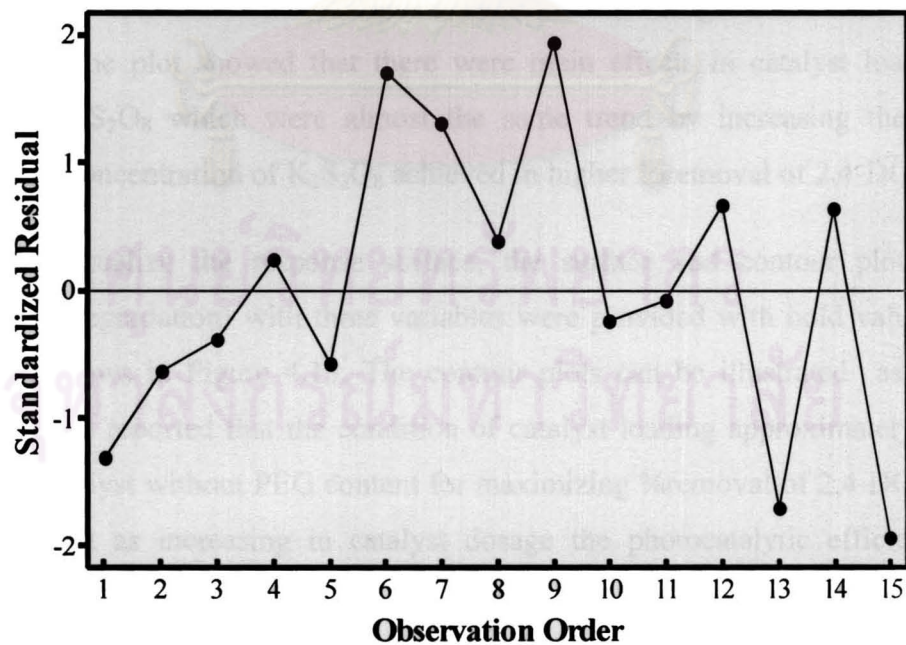


**Figure 4.11** Plot of the standardized residuals in the order of the corresponding observations which fluctuate in a random pattern verified that the designed experiment in which the runs are randomized.

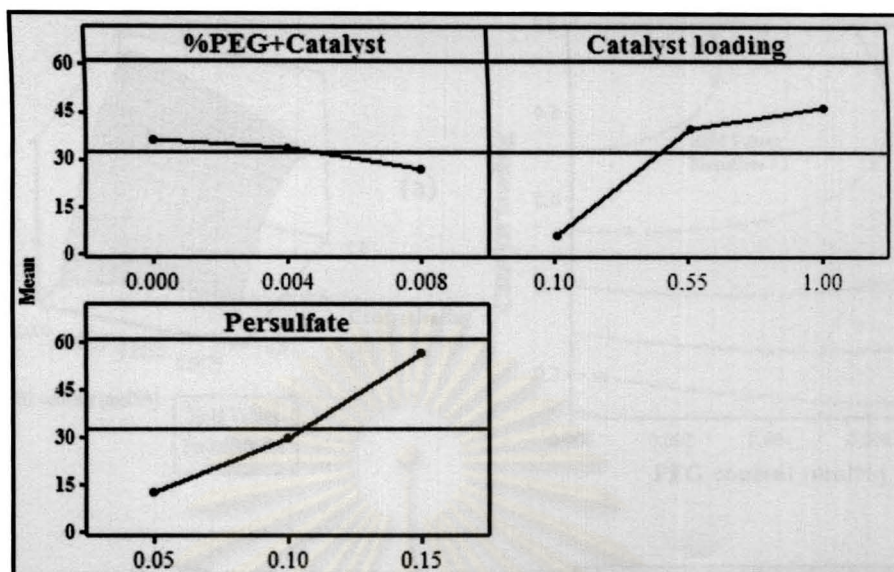


**Figure 4.12** Main effects plot of variables by mean values of %degradation.

The effects of variables by mean values are shown in Figure 4.12. It is noted that PEG contained in photocatalyst had no significant effect to %degradation of 2,4-DCP. As seen from the line, it was almost parallel to an average line (mean = 32.68) and it could be seen that as increase in PEG the mean of %degradation was decreased. In addition, the plot showed that there were main effects in catalyst loading and adding of  $K_2S_2O_8$  which were almost the same trend by increasing the catalyst loading and concentration of  $K_2S_2O_8$  achieved in higher %removal of 2,4-DCP.

To visualize the response surface, the surface and contour plots of the response (%degradation) with three variables were provided with hold values at the middle as shows in Figure 4.13. The contour plots can be illustrated as follows: Figure 4.13(a) reported that the condition of catalyst loading approximately 0.1 g/L and photocatalyst without PEG content for maximizing %removal of 2,4-DCP. It can also note that as increasing in catalyst dosage the photocatalytic efficiency was increased. Figure 4.13(b) shows that the optimum for setting the experiment are 0.15 mM of  $K_2S_2O_8$  and catalyst loading 1 g/L. Figure 4.13(c) indicates that the most suitable for maximizing percentage removal of 2,4-DCP provide at the condition around 0.15 mM of  $K_2S_2O_8$  with the catalyst without PEG content.



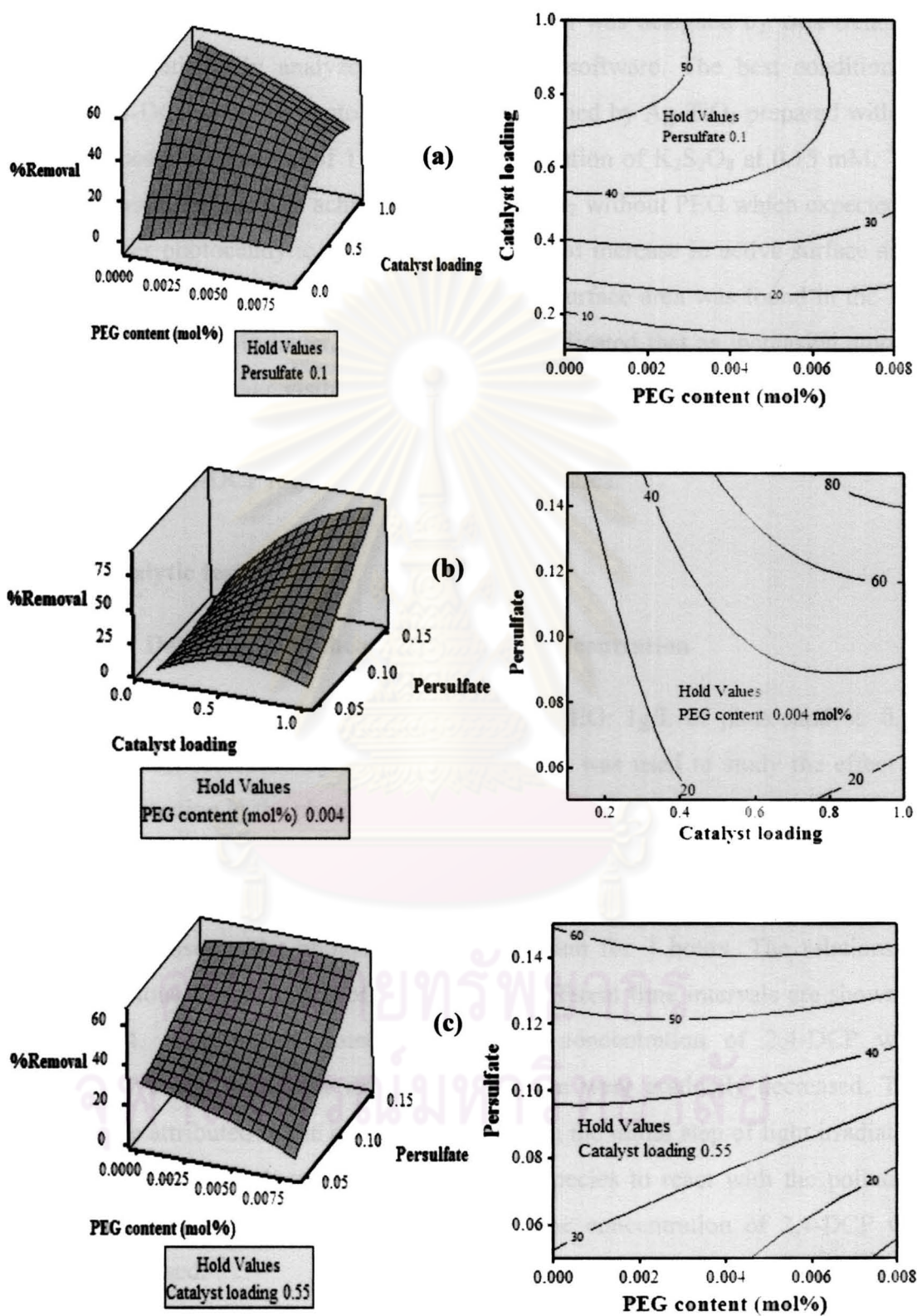


**Figure 4.13** Surface plot of the response (%removal of 2,4-DCP) versus catalyst loading and PEG content (a), catalyst loading and persulfate (b), and PEG content and persulfate.

In summary, the photocatalytic study which was designed by Box-Behnken design and statistically analyzed by Minitab 15 software. The best condition to degrade 2,4-DCP over the photocatalysis was obtained by Ag-TiO<sub>2</sub> prepared without PEG, photocatalyst loading of 1 g/L, and concentration of K<sub>2</sub>S<sub>2</sub>O<sub>8</sub> at 0.15 mM. The smallest crystallite size was achieved in the Ag-TiO<sub>2</sub> without PEG which expected to induce higher photocatalytic performance because of increase in active surface area. In contrast to BET surface area result, the lowest surface area was found in the Ag-TiO<sub>2</sub> without PEG. Moreover, UV-DRS spectra indicated that as increasing amount of PEG results in higher visible light absorption capacity. This small crystallite size of Ag-TiO<sub>2</sub> prepared without PEG would be significant factor for photocatalytic degradation of 2,4-DCP higher than specific surface area.

### **4.3 Photocatalytic testing**

#### **4.3.1 Determination the effect of initial concentration**

The selected condition (Ag-TiO<sub>2</sub> without PEG: 1g/L of photocatalyst: 0.15 mM of K<sub>2</sub>S<sub>2</sub>O<sub>8</sub>) identified by Box-Behnken design was used to study the effect of initial concentration in the photocatalytic degradation of 2,4-DCP at 5, 10, 15, 20, and 25 ppm. The samples were collected after dark condition for an hour to ensure that there were reached adsorption equilibrium. Afterward, sample collection were continued to observe the photocatalytic degradation for 3 hours. The relationship between various concentration of 2,4-DCP and different time intervals are shown in Figure 4.14. It could be noted that at each concentration of 2,4-DCP were significantly decreased in the first 10 minute then were gradually decreased. This result can be attributed to the addition of K<sub>2</sub>S<sub>2</sub>O<sub>8</sub> in the initial step of light irradiation which K<sub>2</sub>S<sub>2</sub>O<sub>8</sub> had produced strongly oxidative species to react with the pollutant. When the oxidative species were not existed, the concentration of 2,4-DCP was steadily decreased.



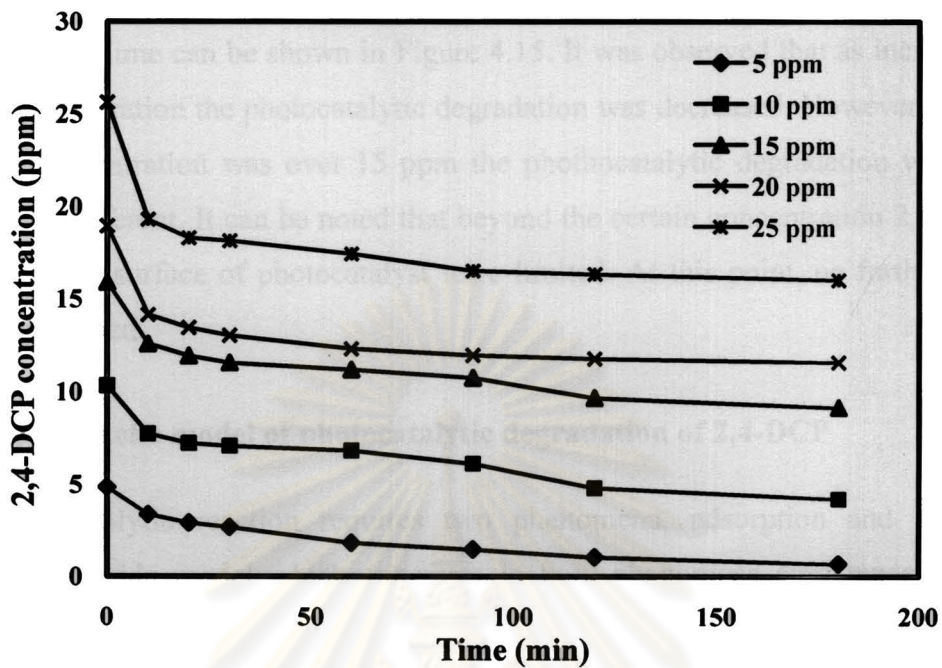


Figure 4.14 Comparison of different initial concentration of 2,4-DCP as a function of time.

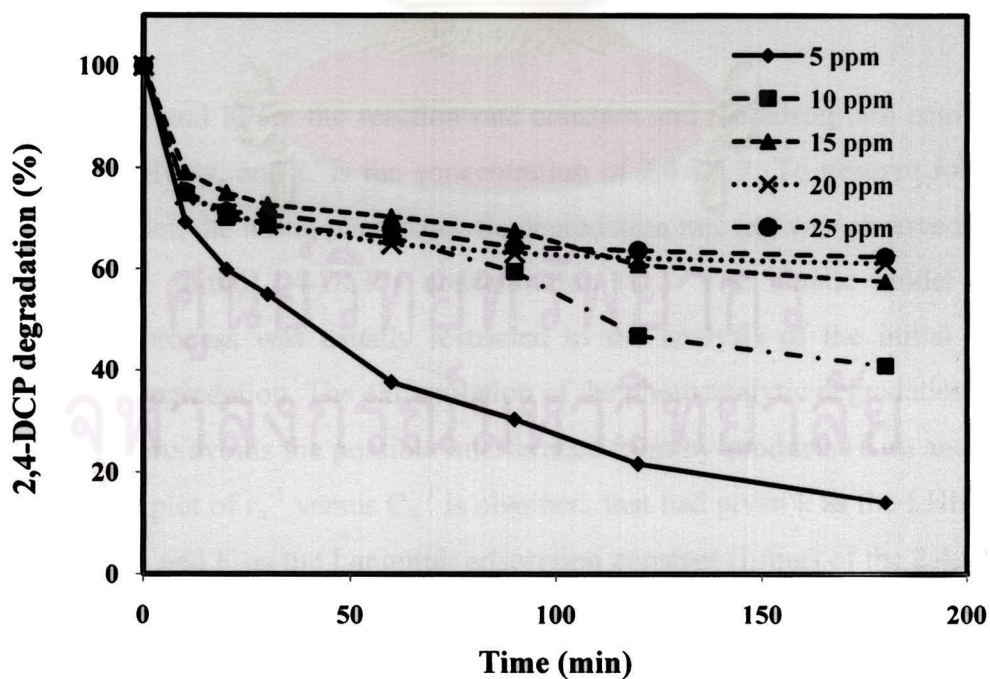


Figure 4.15 Photocatalytic degradation in different initial concentration of 2,4-DCP as a function of time.



The photocatalytic degradation in different initial concentrations of 2,4-DCP as a function of time can be shown in Figure 4.15. It was observed that as increasing in initial concentration the photocatalytic degradation was decreased. However, when the initial concentration was over 15 ppm the photocatalytic degradation was not considerably different. It can be noted that beyond the certain concentration 2,4-DCP adsorbed on the surface of photocatalyst were limited. At this point, no further 2,4-DCP was adsorbed.

#### 4.3.2 Kinetic model of photocatalytic degradation of 2,4-DCP

Photocatalytic reaction requires two phenomena, adsorption and surface reaction. A suitable model which expresses in both phenomena simultaneously is Langmuir-Hinshewood (LHHW) model. According to LHHW model, the reaction rate ( $r$ ) varies proportionally with the surface coverage ( $\theta$ ) as seen in equation (4.4).

$$r = k\theta = \frac{kKC}{1+KC} \quad (4.4)$$

Where  $k$  and  $K$  are the reaction rate constant and the adsorption equilibrium constant respectively, and  $C$  is the concentration of 2,4-DCP. To observe following the LHHW model, the initial photocatalytic degradation rate ( $r_0$ ) was observed to be a function of the initial 2,4-DCP's concentration ( $C_0$ ). The kinetic model of the photocatalytic process was usually restricted to the analysis of the initial rate of photocatalytic degradation. The extrapolation of the photocatalytic degradation rate to time equal to zero avoids the possible interference from by-products (Kim and Hong, 2002). A linear plot of  $r_0^{-1}$  versus  $C_0^{-1}$  is obtained, that had given  $k$  as the LHHW rate constant ( $\text{min}^{-1}$ ) and  $K$  as the Langmuir adsorption constant ( $\text{L/mg}$ ) of the 2,4-DCP in the photocatalytic degradation reaction as shown in equation (4.5) and a linear plot is represented in Figure 4.16.

$$r_0 = \frac{kKC_0}{1+KC_0} \quad \text{or} \quad \frac{1}{r_0} = \frac{1}{kKC_0} + \frac{1}{k} \quad (4.5)$$

The initial photocatalytic degradation rate ( $r_0$ ) ( $\text{min}^{-1}$ ) was determined by numerical method which numerical differentiation formulas can be used when the data points in the independent variable are equally spaced. The three-point differentiation formula at the initial point shows in equation (4.6) (Fogler, 2006). Where  $C$  is concentration at each interested point of time and  $\Delta t$  is the difference of time interval. In kinetic study, the three points; 0 ( $C_{A0}$ ), 10 ( $C_{A1}$ ), and 20 ( $C_{A2}$ ) minutes after light irradiation were used to identify the initial rate of each initial concentration of 2,4-DCP. It was found that the initial rate for 5, 10, 15, 20, and 25 ppm of 2,4-DCP were 0.201, 0.362, 0.468, 0.688, and 0.9  $\text{min}^{-1}$  respectively.

$$r_0 = \left( \frac{dC_A}{dt} \right) = \frac{-3C_{A0} + 4C_{A1} - C_{A2}}{2\Delta t} \quad (4.6)$$

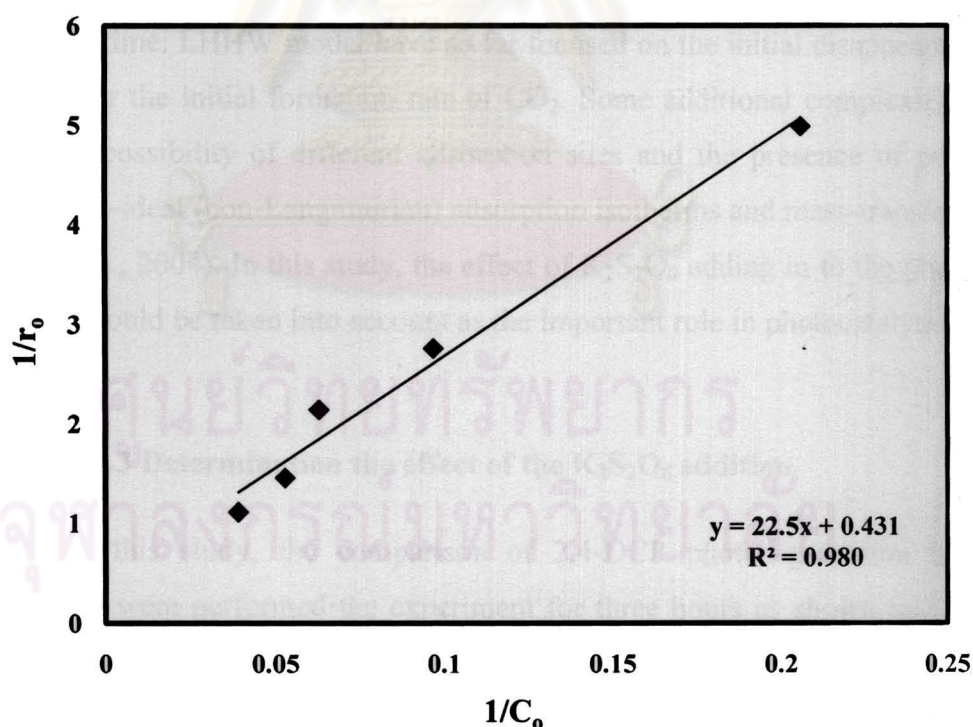


**Figure 4.16** Plot of the reciprocal of the initial rate ( $r_0^{-1}$ ) versus the reciprocal of the initial 2,4-DCP' concentration ( $C_0^{-1}$ ) for photocatalytic degradation of 2,4-DCP.

According to a linear plot in Figure 4.16, the kinetic parameters  $k$  and  $K$  were obtained using linear least squares analysis. The linear plot was represented a good fitting of the model ( $R^2 = 0.98$ ) to the experimental data which indicated that the degradation reaction mechanisms were followed LHHW model. The values of the  $k$  and  $K$  were  $2.3202 \text{ min}^{-1}$  and  $0.0192 \text{ L/mg}$ , respectively. The Langmuir adsorption constant ( $K$ ) was shown that the adsorption reaction was fairly low adsorption in photocatalyst surface.

Considering LHHW model has been regarded as kinetic model for photocatalytic degradation of organic pollutant (Kim and Hong, 2002; Lee et al., 2005). This model successfully explains the kinetics of reactions that occur between two adsorbed species, a free radical and an adsorbed substrate, or a surface bound radical and a free substrate (Carp, Huisman, and Reller, 2004). However, the complex mechanisms of reactions are difficult to develop a model for the dependence of the photocatalytic degradation rate on the experimental parameters for the whole treatment time. LHHW model have so far focused on the initial disappearance rate of organics or the initial formation rate of  $\text{CO}_2$ . Some additional complexity may arise from the possibility of different adsorption sites and the presence of pores, which reflect non-ideal (non-Langmuirian) adsorption isotherms and mass-transfer problems (Carp et al., 2004). In this study, the effect of  $\text{K}_2\text{S}_2\text{O}_8$  adding in to the photocatalytic reaction would be taken into account as the important role in photocatalytic activity.

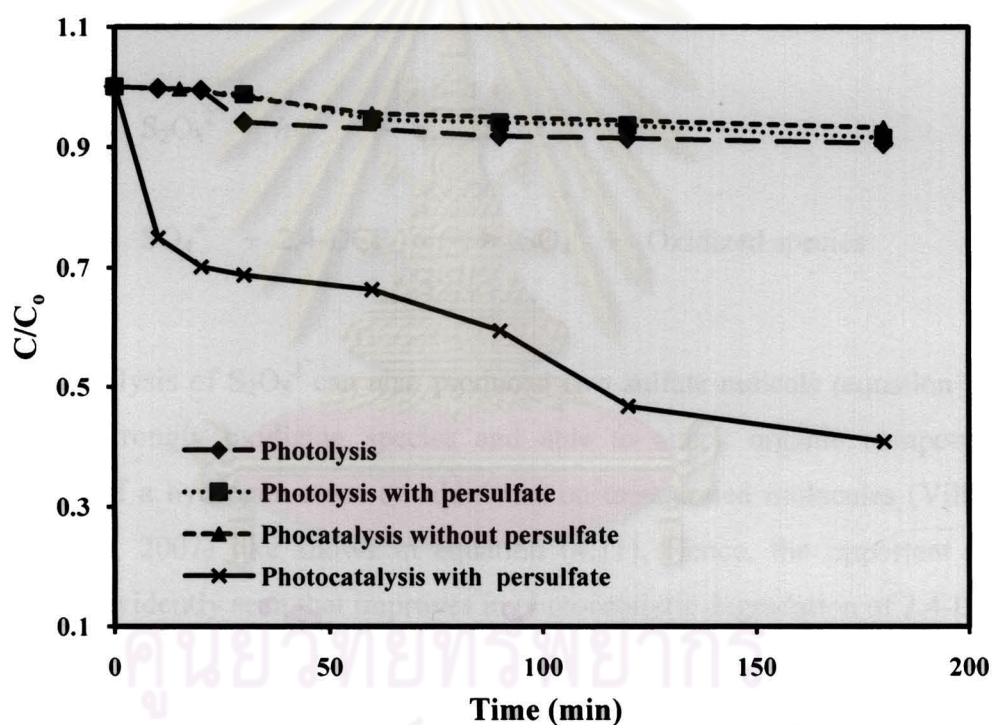
#### 4.3.3 Determination the effect of the $\text{K}_2\text{S}_2\text{O}_8$ addition

In this study, the comparison of 2,4-DCP photodegradation in different conditions were performed the experiment for three hours as shown in Figure 4.17. The photodegradation of 2,4-DCP was compared under different conditions; photolysis, photolysis with  $\text{K}_2\text{S}_2\text{O}_8$ , and photocatalysis without  $\text{K}_2\text{S}_2\text{O}_8$ . The results in %degradation of 2,4-DCP in each condition shows in Table 4.8.



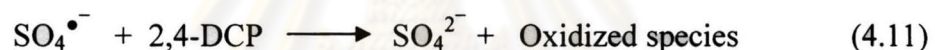
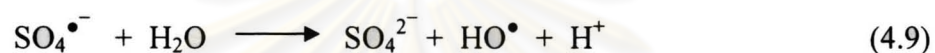
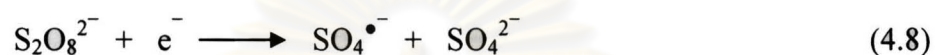
**Table 4.8** Degradation of 2,4-DCP under different conditions.

Condition	% Degradation
Photolysis	10.55
Photolysis with $K_2S_2O_8$	4.24
Photocatalysis without $K_2S_2O_8$	7.25
Photocatalysis with $K_2S_2O_8$	20.71

**Figure 4.17** Photocatalytic degradation of 2,4-DCP at different condition.

As a result in Figure 4.17 and Table 4.8, photocatalysis with  $K_2S_2O_8$  provided the highest photocatalytic degradation which was significant different from that under the photolysis with  $K_2S_2O_8$  and photocatalysis without  $K_2S_2O_8$ . This results indicated that the addition of  $K_2S_2O_8$  was significant effected to the photodegradation of 2,4-DCP. These results were revealed the important role of  $K_2S_2O_8$  to photocatalytic activity. Considering the role of persulfate ion ( $S_2O_8^{2-}$ ), it acted as electron acceptor.

Then reacted with the conduction band electrons photogenerated on the TiO<sub>2</sub> particles and suppressed the efficiency lowering process of electron-hole recombination as illustrated by equation (4.7) and (4.8) (Mills and Valenzuela, 2004). Moreover, the sulfate radical (SO<sub>4</sub><sup>•-</sup>) can further generate hydroxyl radical as shown in equation (4.9).



Photolysis of S<sub>2</sub>O<sub>8</sub><sup>2-</sup> can also produced two sulfate radicals (equation (4.10)), which are strongly oxidizing species and able to attack organic compounds by abstraction of a hydrogen atom or additional on unsaturated molecules (Villanueva and Matínez, 2007) like shows in equation (4.11). Hence, the important role of K<sub>2</sub>S<sub>2</sub>O<sub>8</sub> has evidently seen that improves in photocatalytic degradation of 2,4-DCP.

ศูนย์วิทยทรัพยากร  
จุฬาลงกรณ์มหาวิทยาลัย

# CHAPTER V

## CONCLUSIONS AND RECCOMENDATIONS

### 5.1 Conclusions

The study was divided into two parts. The first one was to synthesis and characterizations of prepared catalysts. Several techniques were used to understand physico-chemical properties of the catalyst. Later on some selected catalysts were tested for the 2,4-DCP photodegradation under visible light. Performance and kinetic evaluations were presented.

In this study, 5 mol% Ag-TiO<sub>2</sub> photocatalysts were prepared via sol-gel method by using polyethylene glycol (PEG) as template. PEG was added in different contents; 0, 0.001, 0.004, and 0.008 mol%. The higher PEG content added into the material, the bigger crystallite size (22-25 nm), the higher visible light absorption capacity, the lower energy band gap (2.46-2.83 eV), and the higher BET surface area (9-14 m<sup>2</sup>/g) could be obtained.

The use of Box-Behnken design based on design of experiments (DOEs) was applied to determine the operating condition for maximizing 2,4-DCP photodegradation. Three parameters were taken into account of this study. There were amount of PEG, photocatalyst loading, and concentration of K<sub>2</sub>S<sub>2</sub>O<sub>8</sub>. The series of batch tests was conducted randomize following the experimental design. The highest photocatalytic activity for removal of 2,4-DCP was achieved at Ag-TiO<sub>2</sub> without PEG suspended in 0.1 g/L of photocatalyst and 0.15 mM of K<sub>2</sub>S<sub>2</sub>O<sub>8</sub>. PEG content had no significant statistically effect to photocatalytic degradation of 2,4-DCP. This condition was further used to evaluate the kinetic parameters of Langmiur-Hinsewood (LHHW) model. The result was followed LHHW model which the LHHW rate constant (k) and Langmuir adsorption constant (K) were 2.3202 min<sup>-1</sup> and 0.0192 L/mg respectively.



## 5.2 Recommendations

- Application of Ag-TiO<sub>2</sub> photocatalysts synthesized using PEG as template for other organic pollutants, such as soluble volatile organic compounds, should be included and differentiated the performance of each.
- It is interesting to investigate how to improve the photocatalytic efficiency of Ag-TiO<sub>2</sub> photocatalysts by synthesizing with other templates or other synthesis method to obtain surface area more than P25 -TiO<sub>2</sub> commercial (51 m<sup>2</sup>/g).
- Investigation on how to improve the photocatalytic efficiency without the addition of an oxidant or the addition of other oxidants.
- More parameter such as light intensity should be added in the interaction effects for the next concern.

## REFERENCES

- Agency for toxic substances and disease registry. 2009. Minimal risk levels (MRLs) for hazardous substances [Online]. Available from: <http://www.atsdr.cdc.gov/mrls/mrllists/.asp> [2010, January 10]
- Arconada, N et al. 2009. Synthesis and photocatalytic properties of dense and porous TiO<sub>2</sub>-anatase thin films prepared by sol-gel. Applied catalysis B: Environmental 86: 1-7.
- Bao xiu, Z., Xiang-zhong, LI., and Peng, W. 2007. Degradation of 2,4-dichlorophenol with a novel TiO<sub>2</sub>/Ti-Fe-graphite felt photoelectrocatalytic oxidation process. Journal of environmental sciences 19: 1020-1024.
- Boonyatumanond, R., Jaksakul, A., Boonchalermkit, S., Pucharoen, P., and Tabucanon, M.S. 2001. Monitoring of endocrine disruptor compounds in the coastal hydrosphere of Thailand [online]. Available from: <http://landbase-hq.unu.edu/Monitoring/Countryreports/Thailand/final%20data%20report%20UNU.htm> [2009, September 2]
- Brigden, K., Labunska, I., and Stringer, R. 2003. The Bangpoo industrial estate, Samut-Prakan province, Thailand; An investigation of environmental pollutants[Online]. Available from: <http://www.greenpeace.to/publications/Bangpoo2003.pdf> [2009, August 5]
- Bu, S.J., Jin, Z.G., Liu, X.X., Yang, L.R., and Cheng, Z.J. 2005. Synthesis of TiO<sub>2</sub> porous thin films by polyethylene glycol templating and chemistry of the process. Journal of the European Ceramic Society 25: 673-679.
- Carp, O., Huisman, C.L., and Reller, A. 2004. Photoinduced reactivity of titanium dioxide. Progress in Solid State Chemistry 32: 33-177.
- Chang, M.Y. et al. 2009. Photocatalytic degradation of 2,4-dichlorophenol wastewater using porphyrin/TiO<sub>2</sub> complexes activated by visible light. Thin solid films 517:3888-3891.
- Chao, H.E., Yun, Y.U., Xingfang, H.U., and Larbot, A. 2003. Effect of silver doping on the phase transformation and grain growth of sol-gel titania powder. Journal of the European Ceramic Society 23: 1457-1464.

- Chatterjee, D. and Dasgupta, S. 2005. Visible light induced photocatalytic degradation of organic pollutants. Journal of Photochemistry and Photobiology C: Photochemistry reviews 6: 186-205.
- Chen, X. and Mao, S.S. 2007. Titanium dioxide nanomaterials: synthesis, properties, modifications, and applications. Chemical reviews 107 (7): 2891-2959.
- Daneshvar, N., Salari, D., and Khataee, A.R. 2003. Photocatalytic degradation of azo dye acid red 14 in water: investigation of the effect of operational parameters. Journal of Photochemistry and Photobiology A: Chemistry 157: 111-116.
- Diebold, U. 2003. The surface science of titanium dioxide. Surface science reports 48: 53-229.
- Estevinho, B.N., Martins, I., Ratola, N., Alves, A., and Santos, L. 2007. Removal of 2,4-dichlorophenol and pentachlorophenol from waters by sorption using coal fly ash from a Portuguese thermal power plant. Journal of hazardous materials 143: 535-540.
- Fogler, H.S. 2006. Element of chemical reaction engineering. Fourth edition. United States of America: Person education publication.
- Gaya, U.I. and Abdullah, A.H. 2008. Heterogeneous photocatalytic degradation of organic contaminants over titanium dioxide: A review of fundamentals, progress and problems. Journal of Photochemistry and Photobiology C: Photochemistry Reviews 9: 1-12.
- Ghanem, K.M., Al-Garni, S.M., and Al-Shehri, A.N. 2009. Statistical optimization of cultural conditions by response surface methodology for phenol degradation by a novel *Aspergillus flavus* isolate. African Journal of Biotechnology Vol. 8 (15): 3576-3583.
- Guo, B., Liu, Z., Hong, L., and Jiang, H. 2005. Sol gel derived photocatalytic porous TiO<sub>2</sub> thin films. Surface & Coatings Technology 198: 24-29.
- Herrmann, J.M. 1999. Heterogeneous photocatalysis: fundamentals and applications to the removal of various types of aqueous pollutants. Catalyst today 53: 115-129.



- Hoffmann, M.R., Martin, S.T., Choi, W., and Bahnemann, D.W. 1995. Environmental applications of semiconductor photocatalysis. Chemical reviews 95 (1): 69-96.
- Jiao, J., Xu, Q., Li, L., Tsubasa, T., and Kobayashi, T. 2008. Effect of PEG with different M W as template direction reagent on preparation of porous TiO<sub>2</sub>-SiO<sub>2</sub> with assistance of supercritical CO<sub>2</sub>. Colloid Polymer Science 286: 1485-1491.
- Kaneko, M. and Okura, I. 2002. Photocatalysis. Japan: Springer.
- Kim, S.B. and Hong, S.C. 2002. Kinetic study for photocatalytic degradation of volatile organic compounds in air using thin film TiO<sub>2</sub> photocatalyst. Applied Catalysis B: Environmental 35: 305-315.
- Lasa, H., Serrano, B., and Salaices, M. 2005. Photocatalytic engineering. United States of America: Springer.
- Lee, M.S., Hong, S.S., and Mohseni, M. 2005. Synthesis of photocatalytic nanosized TiO<sub>2</sub>-Ag particles with sol-gel method using reduction agent. Journal of molecular catalysis A: Chemical 242: 135-140.
- Linsebigler, A.L. 1995. Photocatalysis on TiO<sub>2</sub> surfaces: Principles, mechanisms, and selected results. Chemical reviews 95 (3): 735-758.
- Liu, S.X., Qu, Z.P., Han, X.W., and Sun, C.L. 2004. A mechanism for enhanced photocatalytic activity of silver-loaded titanium dioxide. Catalysis today 93-95: 877-884.
- Milla, A. and Valenzuela, M.A. 2004. The photo-oxidation of water by sodium persulfate and other electron acceptors, sensitized by TiO<sub>2</sub>. Journal of Photochemistry and Photobiology A: Chemistry 165: 25-34.
- Murphy, A.B. 2007. Band-gap determination from diffuse reflectance measurements of semiconductor films and application to photoelectrochemical water-splitting. Solar Energy Materials & Solar Cells 91:1326-1337.
- Ormad, M.P., Ovelleiro, J. L., and Kiwi, J. 2001. Photocatalytic degradation of concentrated solutions of 2,4-dichlorophenol using low energy light identification of intermediates. Applied Catalysis B: Environmental 32: 157-166.

- Pera-Titus, M., Garc'ia-Molina, V., Baños, M.A., Giménez, J., and Espluga, S. 2004. Degradation of chlorophenols by means of advanced oxidation processes. Applied Catalysis B: Environmental 47: 219-256.
- Pure Green Protective Coatings (PGC). 2009. How does PGC Pure Green Protective Coatings Work. Photocatalytic process [Online]. Available from: [http://puregreencoatings.com/pgc\\_science.aspx](http://puregreencoatings.com/pgc_science.aspx) [2009, August 3]
- Qiu, S. and Kalita, S.J. 2006. Synthesis, processing and characterization of nanocrystalline titanium dioxide. Materials science and engineering A 435-436: 327-332.
- Ren, S. and Frymier, P.D. 2002. Estimating the toxicities of organic chemicals to bioluminescent bacteria and activated sludge. Water Research 36: 4406-4414.
- Ray, S., Lalman, J.A., Biswas, N. 2009. Using the Box-Benken technique to statistically model phenol photocatalytic degradation by titanium dioxide nanoparticles. Chemical Engineering Journal 150: 15-24.
- Sakthivel, S. et al. 2004. Enhancement of photocatalytic activity by metal deposition: characterisation and photonic efficiency of Pt, Au and Pd deposited on TiO<sub>2</sub> catalyst. Water Research 38: 300-3008.
- Seery, M.K., George, R., Floris, P., Pillai, and Suresh, C. 2007. Silver doped titanium dioxide nanomaterials for enhanced visible light photocatalysis. Journal of Photochemistry and Photobiology A: Chemistry 189: 258-263.
- U.S. Department of health and human services. Agency for toxic substances and disease registry. 1999. Toxicological profile for chlorophenol [Online]. Available from: <http://www.atsdr.cdc.gov/toxprofiles/tp107.html> [2009, August 10]
- U.S. Environmental Protection Agency. Clean Water Act. 2008. Priority pollutants [Online]. Available from: <http://www.epa.gov/waterscience/methods/pollutants.htm> [2009, August 10]
- Villanueva, S.F. and Mat'inez, S.S. 2007. TiO<sub>2</sub> assisted degradation of acid orange 7 textile dye under solar light. Solar energy materials & solar cells 91: 1492-1495.

- Wang, H. and Wang, J. 2008. Electrochemical degradation of 2,4-dichlorophenol on a palladium modified gas-diffusion electrode. Electrochimica acta 53: 6402-6409.
- Wang, H. and Wang, J. 2009. Comparative study on electrochemical degradation of 2,4-dichlorophenol by different Pd-C gas-diffusion cathodes. Applied catalysis B: Environmental 89: 111-117.
- Xin, B., Jing, L., Ren, Z., Wang, B., and Fu, H. 2005. Effects of simultaneously doped and deposited Ag on the photocatalytic activity and surface states of TiO<sub>2</sub>. Journal physical chemistry B 109 (7): 2805-2809.
- Yasman, Y., Bulatov, V., Rabin, I., Binetti, B., and Schechter, I. 2006. Enhanced electro-catalytic degradation of chloroorganic compounds in the presence of ultrasound. Ultrasonics Sonochemistry 13: 271-277.
- Yu, K. et al. 2005. Sol-gel synthesis and hydrothermal processing of anatase nanocrystals from titanium n-butoxide. Materials letters 59: 2515-2518.
- Zhang, L., Zhu, Y., Hu, Y., Li, W., and Sun, H. 2003. Preparation and performances of mesoporous TiO<sub>2</sub> film photocatalyst supported on stainless steel. Applied Catalysis B: Environmental 40: 287-292.





**APPENDIX**

ศูนย์วิทยทรัพยากร  
จุฬาลงกรณ์มหาวิทยาลัย

# 1. Determination of band gap from absorption coefficient by Kubelka-Munk

## Model

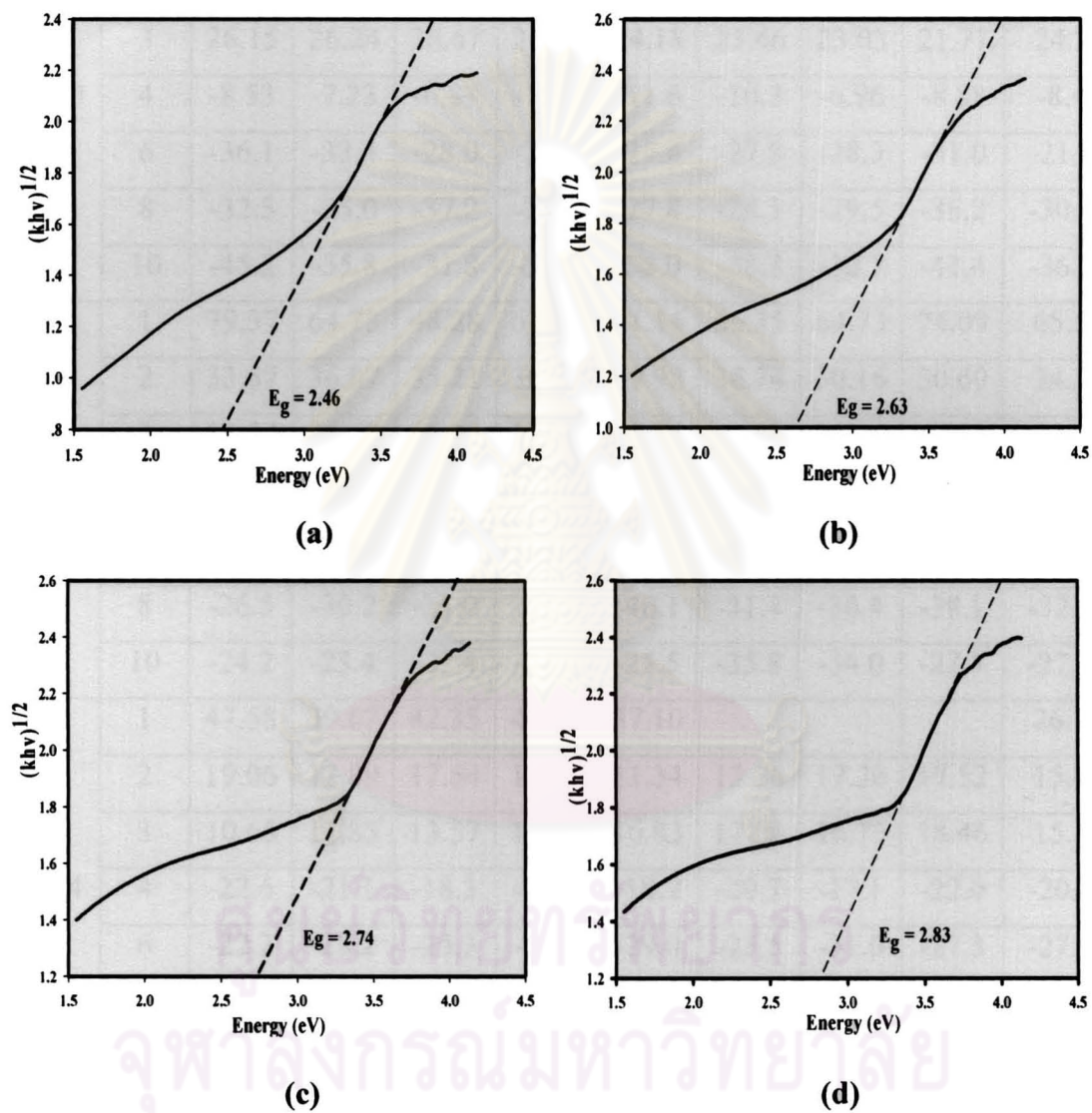


**Figure A.1** Energy band gap of Ag-TiO<sub>2</sub> without PEG(a), 0.001 mol% PEG(b), 0.004 mol% PEG(c), and 0.008 mol% PEG(d).

## 2. Determination of point of zero charge from Zeta potential

**Table A.1** Zeta potential results of Ag-TiO<sub>2</sub> with difference mol% of PEG.

Mol% PEG	pH	Replicate								Average
		1	2	3	4	5	6	7	8	
0.000	1	56.82	62.13	66.14	58.79	44.82	67.07	53.71	45.97	59.13
	2	92.27	88.47	88.79	78.34	79.29	75.19	64.80	71.69	79.85
	3	26.15	26.24	26.67	22.80	24.18	23.46	23.03	21.77	24.29
	4	-8.53	-7.23	-6.83	-7.08	-11.6	-10.3	-6.96	-8.88	-8.42
	6	-36.1	-33.4	-28.0	-25.8	-27.4	-27.8	-28.3	-31.0	-21.04
	8	-32.5	-25.0	-37.2	-24.7	-27.8	-28.1	-29.5	-36.2	-30.13
	10	-45.2	-35.8	-31.8	-30.6	-38.0	-38.3	-30.7	-41.4	-36.48
0.001	1	79.37	64.73	48.28	61.80	51.14	56.35	64.73	74.09	65.56
	2	33.57	36.07	35.21	30.67	39.92	36.74	30.16	30.60	34.12
	3	24.54	26.57	26.24	22.69	25.75	25.66	24.80	17.50	24.22
	4	-23.3	-22.7	-26.4	-19.5	-17.2	-25.2	-29.3	-25.3	-23.61
	6	-28.2	-28.4	-26.1	-23.1	-24.7	-31.2	-20.4	-33.8	-26.99
	8	-26.5	-30.2	-31.0	-27.6	-40.1	-31.4	-36.4	-38.1	-32.66
	10	-24.2	-23.4	-22.4	-29.2	-25.5	-35.8	-34.0	-27.7	-27.78
0.004	1	47.58	39.67	42.35	46.99	37.10				26.71
	2	19.06	12.89	17.54	14.51	11.34	13.76	17.26	17.52	15.49
	3	10.66	11.85	13.57	16.81	16.83	17.04	16.73	18.46	15.18
	4	-22.6	-21.1	-18.3	-21.8	-18.9	-20.7	-17.1	-22.0	-20.31
	6	-22.2	-28.2	-25.3	-28.4	-29.0	-25.5	-31.6	-27.3	-27.19
	8	-23.7	-22.4	-24.4	-23.8	-32.9	-17.1	-21.8	-29.6	-24.46
	10	-51.4	-41.3	-51.4	-38.5	-37.4	-33.4	-51.0	-34.9	-42.41
0.008	1	2.804	2.703	2.085	2.890	2.218	1.265	2.585		2.364
	2	28.53	20.07	25.66	30.94	27.00	20.74	21.96	20.86	18.57
	3	28.75	20.77	24.16	24.01	17.02	24.13	23.07	24.76	17.01
	4	-28.4	-26.8	-26.2	-22.9	-25.0	-23.8	-26.1	-23.9	-25.39
	6	-19.1	-25.4	-29.2	-18.5	-22.1	-23.8	-20.9	-21.2	-22.53
	8	-23.9	-23.1	-17.5	-22.0	-20.0	-30.7	-28.6	-26.1	-23.99
	10	-32.7	-35.8	-35.1	-37.4	-40.3	-40.9	-43.6	-41.3	-38.39



### 3. Calibration curve of 2,4-DCP

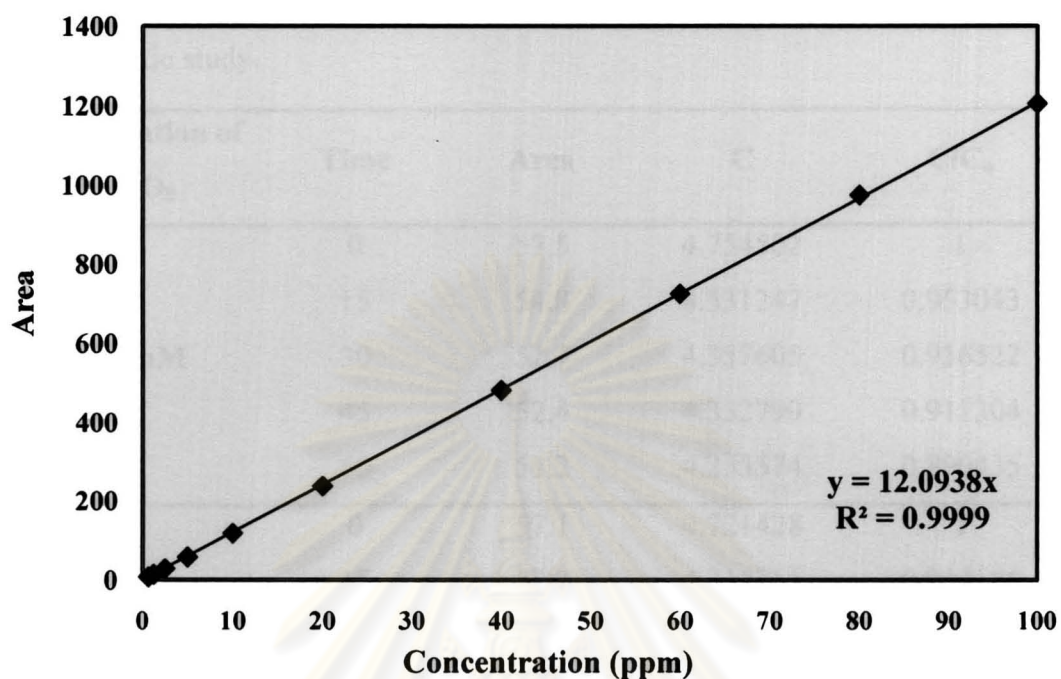


**Figure A.2** Calibration curve plot of peak area as a function of 2,4-DCP concentration.

**Table A.2** Different concentrations were obtained from peak area analyzed by HPLC for calibration curve of 2,4-DCP.

Standard number	Concentration (ppm)	Peak area
1	0.625	7.1
2	1.25	13.6
3	2.5	28.4
4	5	57.3
5	10	117.7
6	20	237.5
7	40	480.6
8	60	725.1
9	80	975.6
10	100	1205.9

#### 4. Kinetic study

**Table A.3** Determination the concentration of  $K_2S_2O_8$  analyzed by HPLC for photodcatalytic study.

Concentration of $K_2S_2O_8$	Time	Area	C	C/C <sub>0</sub>
0.05 mM	0	57.5	4.754502	1
	15	54.8	4.531247	0.953043
	30	52.7	4.357605	0.916522
	45	52.4	4.332799	0.911304
	60	51.2	4.233574	0.890435
	0.10 mM	0	57.1	4.721428
15		52.2	4.316261	0.914186
30		51.8	4.283186	0.90718
45		51.2	4.233574	0.896673
60		50.1	4.142619	0.877408
0.25 mM		0	55.7	4.605666
	15	35	2.894045	0.628366
	30	34.7	2.869239	0.62298
	45	30.9	2.555028	0.554758
	60	0	0	0
	0.50 mM	0	58.1	4.804115
15		0	0	0
30		0	0	0
45		0	0	0
60		0	0	0
0.75 mM		0	56.6	4.680084
	15	0	0	0
	30	0	0	0
	45	0	0	0
	60	0	0	0

**Table A.4** Determination the effect of initial concentration for kinetic study was analyzed by HPLC.

5 ppm				10 ppm			
Time	Area	C	C/C <sub>0</sub>	Time	Area	C	C/C <sub>0</sub>
0	58.7	4.853727	1	0	124.8	10.31934	1
10	40.7	3.365361	0.693356	10	93.6	7.739503	0.75
20	35.2	2.910582	0.599659	20	87.6	7.243381	0.701923
30	32.3	2.67079	0.550256	30	85.8	7.094544	0.6875
60	22.1	1.827383	0.376491	60	82.8	6.846483	0.663462
90	17.8	1.471829	0.303237	90	74.3	6.143644	0.595353
120	12.73	1.052605	0.216865	120	58.4	4.828921	0.467949
180	8.3	0.686302	0.141397	180	51	4.217037	0.408654

15 ppm				20 ppm			
Time	Area	C	C/C <sub>0</sub>	Time	Area	C	C/C <sub>0</sub>
0	192.2	15.89244	1	0	229.1	18.94359	1
10	152	12.56842	0.790843	10	170.9	14.13121	0.7459625
20	144.3	11.93173	0.75078	20	162.6	13.44491	0.7097337
30	139.8	11.55964	0.727367	30	157.6	13.03147	0.6879092
60	135.3	11.18755	0.703954	60	148.9	12.31209	0.6499345
90	130.1	10.75758	0.676899	90	144.8	11.97308	0.6320384
120	117	9.674379	0.608741	120	142.6	11.79117	0.6224356
180	110.7	9.153451	0.575963	180	140.2	11.59272	0.6119598

25 ppm			
Time	Area	C	C/C <sub>0</sub>
0	310	25.63297	1
10	233.4	19.29915	0.7529032
20	221.3	18.29863	0.713871
30	219.4	18.14153	0.7077419
60	210.8	17.43042	0.68
90	199.7	16.51259	0.6441935
120	197.5	16.33068	0.6370968
180	193.7	16.01647	0.6248387



## BIOGRAPHY

Miss Sineenat Unburee was born on 10<sup>th</sup> January, 1986 in Roi-Et, Thailand. In March 2004, she finished high school at Sarakham Pittayakom School, Mahasarakham, Thailand. Afterward, she obtained her B.Sci (Health Sci) major in environmental health in academic year 2004 and graduated in March, 2007. In February 2008, the National Center of Excellence for Environmental and Hazard Waste Management (NCE-EHWM) gave her opportunity to learn with full scholarship in International Postgraduate Programs in Environmental Management, Chulalongkorn University. She is interested in the field of photocatalysis, hazardous waste management, waste water treatment, and climate change.



ศูนย์วิทยทรัพยากร  
จุฬาลงกรณ์มหาวิทยาลัย